Zonally dominated saturation and Dimits phase transition in curvature-driven ITG turbulence

P. G. Ivanov[1,2], A. A. Schekochihin[1],
W. Dorland[1,3], A. R. Field[2], F. I. Parra[1]

[1] *Rudolf Peierls Centre for Theoretical Physics, University of Oxford, Oxford OX1 3PU, UK*

[2] *EURATOM/UKAEA Fusion Association, Culham Science Centre, Abingdon, OX14 3DB, UK*

[3] *Department of Physics, University of Maryland, College Park, Maryland 20740, USA*

Overview

- Understanding heat transport in tokamak plasmas is crucial for the design of future experiments and reactors
- Numerical evidence points towards turbulence as the main cause for heat transport in tokamak plasmas
- Therefore, we seek to describe the saturated turbulent state and the mechanisms of its saturation
- We focus on turbulence driven by the ion-temperature-gradient (ITG) instability

Outline

- ITG saturation, zonal flows (ZFs) and the Dimits shift
- 2D 2-fluid magnetic-curvature-driven ITG model
  - Naturally capture the ITG microinstability
  - This model has a well-defined Dimits transition
- We investigate the character of near-marginal turbulence and the saturation mechanisms
  - The near-marginal state is dominated by quasi-static strong zonal flows
  - Intertwined patch-wise constant zonal shear and strong zonal temperature perturbations, somewhat reminiscent of the $\boldsymbol{E} \times \boldsymbol{B}$ staircase (Dif-Pradalier *et al.*, 2010)
- By considering the zonal flow drive in this state, we find an analytical estimate for the Dimits threshold

The Dimits shift

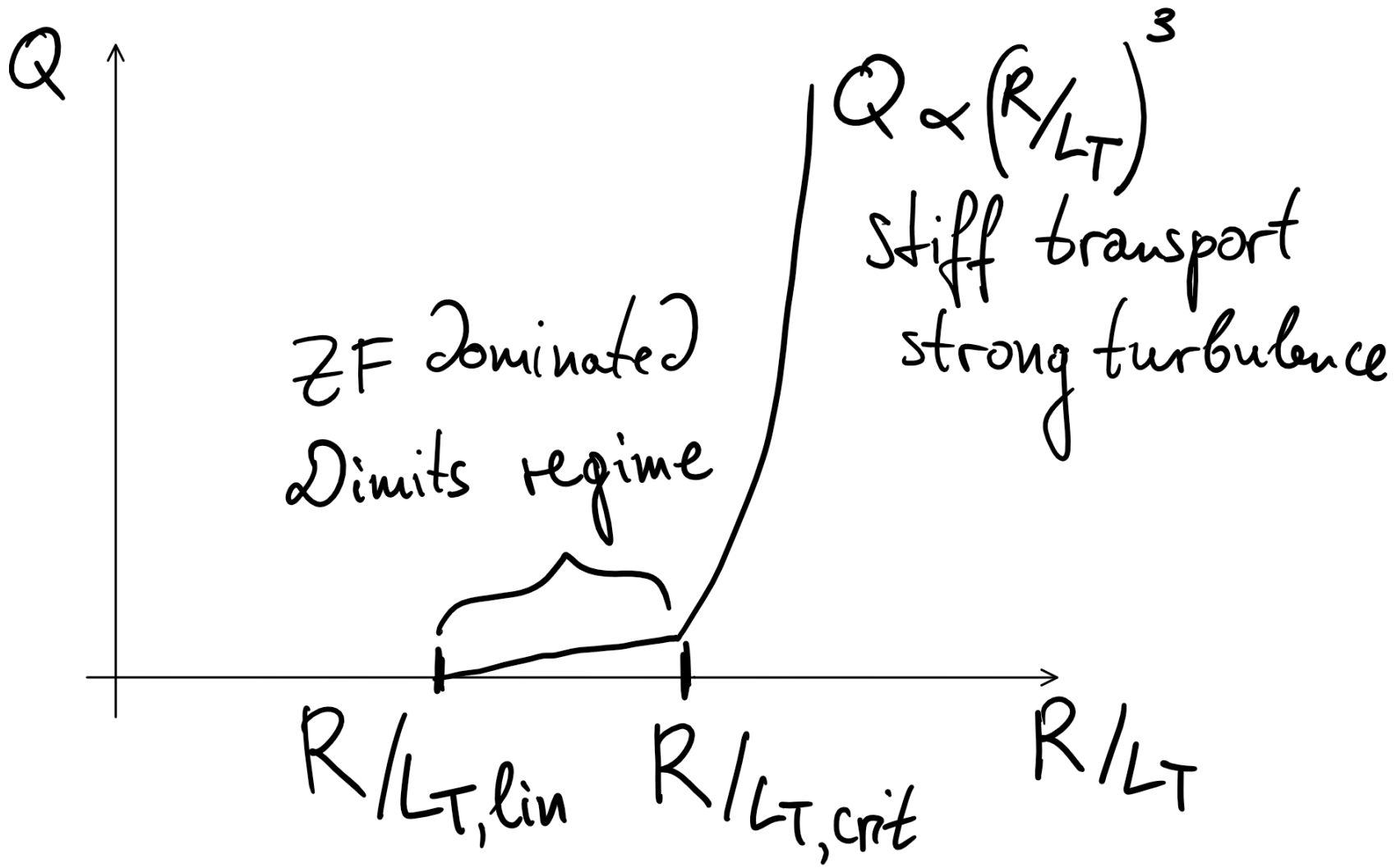

Figure 1: The Dimits shift paradigm (Dimits *et al.*, 2000).

How do we approach this?

- We use a 2D 2-field model for the perturbations of electrostatic potential and ion temperature
- Derived in a physically realisable, if not necessary most general, regime as an asymptotic limit of the electrostatic ion gyrokinetic (GK) equation
- Contains a curvature-driven ion-temperature-gradient (ITG) microinstability, characteristic of tokamak plasmas
- A two-field model allows us to capture the important ITG linear instability, while keeping the equations simple enough for analytic progress to be possible
- We find that this model has a well-defined Dimits transition

Geometry

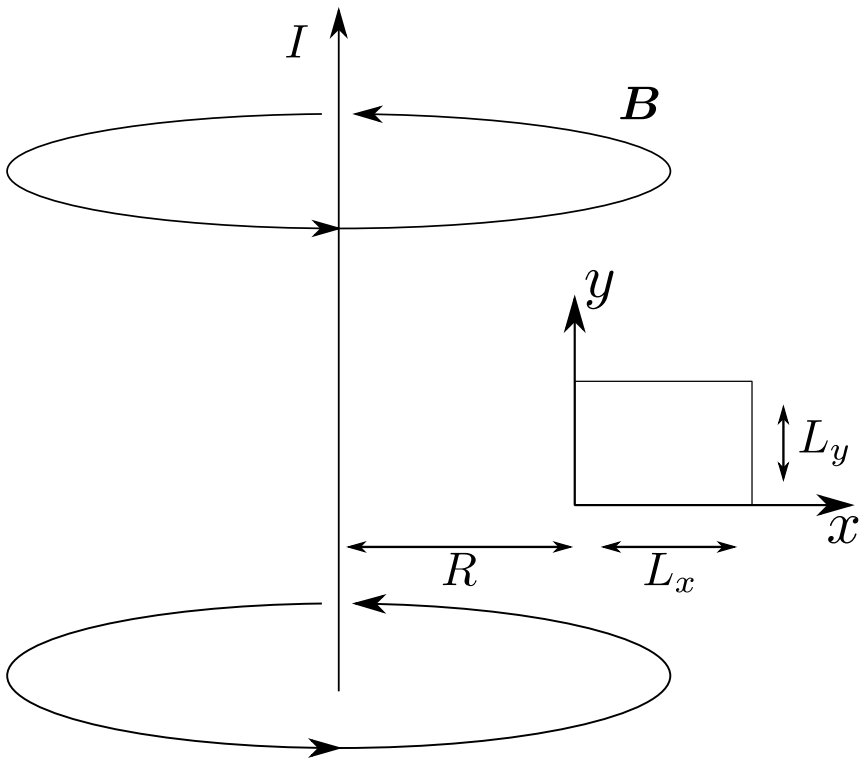

Figure 2: Illustration of the Z-pinch magnetic geometry. Here x and y correspond to the "radial" and "poloidal" coordinates in a tokamak.

$$L_B^{-1} \equiv -\frac{1}{B}\frac{dB}{dx}, \qquad L_T^{-1} \equiv -\frac{1}{T_i}\frac{dT_i}{dx} \tag{1}$$

Electron response

- Electron physics — modified adiabatic response:

$$\frac{\delta n_e}{n_e} = \frac{e(\phi - \overline{\phi})}{T_e} = \frac{e\phi'}{T_e}, \tag{2}$$

  where $\overline{\phi}$ is the flux-surface (zonal) average of the electrostatic potential ϕ and $\phi' \equiv \phi - \overline{\phi}$ is the nonzonal part of the field

- This electron response has been found to be crucial for capturing essential zonal-flow properties (Hammett *et al.*, 1993)

Orderings

- Highly-collisional, long-wavelength, 2D ($k_\parallel = 0$) limit

$$\nu_i \gg \partial_t \sim k_\perp^2 \rho_i^2 \nu_i, \qquad k_\perp^2 \rho_i^2 \ll 1. \tag{3}$$

- Cold ions $T_i/T_e \to 0$, but finite sound radius

$$\rho_s \equiv \frac{\rho_i}{\sqrt{2\tau}}, \ \tau \equiv \frac{T_i}{ZT_e}. \tag{4}$$

Applying these approximations to the ion gyrokinetic (GK) equation, we obtain a system of closed equations for the electric potential ϕ and ion temperature perturbations δT_i.

Normalised equations

$$\partial_t \left(\varphi' - \nabla^2\varphi\right) + \left\{\varphi, \varphi' - \nabla^2\varphi\right\} + \nabla \cdot \{\nabla\varphi, T\}$$
$$-\partial_y \left(\varphi + T\right) + \kappa_T \partial_y \nabla^2 \varphi = -\chi \nabla^4 (a\varphi - bT), \tag{5}$$

$$\partial_t T + \{\varphi, T\} + \kappa_T \partial_y \varphi = \chi \nabla^2 T. \tag{6}$$

The only parameters are κ_T, χ and the size of the domain L_x, L_y.

$$\kappa_T \equiv \frac{\tau L_B}{2L_T}, \qquad \chi \equiv \frac{\tau L_B}{\rho_s} \frac{8}{9} \sqrt{\frac{2}{\pi}} \frac{\nu_i}{\Omega_i} \tag{7}$$

Normalised equations

$$\partial_t \left(\varphi' - \nabla^2\varphi\right) + \left\{\varphi, \varphi' - \nabla^2\varphi\right\} + \nabla \cdot \left\{\nabla\varphi, T\right\}$$
$$-\partial_y \left(\varphi + T\right) + \kappa_T \partial_y \nabla^2 \varphi = -\chi \nabla^4 (a\varphi - bT), \tag{5}$$

$$\partial_t T + \left\{\varphi, T\right\} + \kappa_T \partial_y \varphi = \chi \nabla^2 T. \tag{6}$$

Ion density perturbation: $\partial_t \left(\varphi' - \nabla^2\varphi\right)$

Normalised equations

$$\partial_t \left(\varphi' - \nabla^2\varphi\right) + \left\{\varphi, \varphi' - \nabla^2\varphi\right\} + \nabla \cdot \{\nabla\varphi, T\}$$
$$-\partial_y \left(\varphi + T\right) + \kappa_T \partial_y \nabla^2 \varphi = -\chi \nabla^4 (a\varphi - bT), \tag{5}$$

$$\partial_t T + \{\varphi, T\} + \kappa_T \partial_y \varphi = \chi \nabla^2 T. \tag{6}$$

$\boldsymbol{E} \times \boldsymbol{B}$ advection of ion density: $\left\{\varphi, \varphi' - \nabla^2\varphi\right\}$

Normalised equations

$$\partial_t \left(\varphi' - \nabla^2\varphi\right) + \left\{\varphi, \varphi' - \nabla^2\varphi\right\} + \nabla \cdot \{\nabla\varphi, T\}$$
$$-\partial_y \left(\varphi + T\right) + \kappa_T \partial_y \nabla^2 \varphi = -\chi \nabla^4 (a\varphi - bT), \tag{5}$$

$$\partial_t T + \{\varphi, T\} + \kappa_T \partial_y \varphi = \chi \nabla^2 T. \tag{6}$$

FLR nonlinear term: $\nabla \cdot \{\nabla\varphi, T\}$

Normalised equations

$$\partial_t \left(\varphi' - \nabla^2\varphi\right) + \left\{\varphi, \varphi' - \nabla^2\varphi\right\} + \nabla \cdot \{\nabla\varphi, T\}$$
$$-\partial_y \left(\varphi + T\right) + \kappa_T \partial_y \nabla^2 \varphi = -\chi \nabla^4 (a\varphi - bT), \tag{5}$$

$$\partial_t T + \{\varphi, T\} + \kappa_T \partial_y \varphi = \chi \nabla^2 T. \tag{6}$$

Magnetic drift: $-\partial_y \left(\varphi + T\right)$

Normalised equations

$$\partial_t \left(\varphi' - \nabla^2\varphi\right) + \left\{\varphi, \varphi' - \nabla^2\varphi\right\} + \nabla \cdot \{\nabla\varphi, T\}$$
$$-\partial_y \left(\varphi + T\right) + \kappa_T \partial_y \nabla^2 \varphi = -\chi \nabla^4 (a\varphi - bT), \tag{5}$$

$$\partial_t T + \{\varphi, T\} + \kappa_T \partial_y \varphi = \chi \nabla^2 T. \tag{6}$$

Diamagnetic drift: $\kappa_T \partial_y \nabla^2 \varphi$

Normalised equations

$$\partial_t \left(\varphi' - \nabla^2\varphi\right) + \left\{\varphi, \varphi' - \nabla^2\varphi\right\} + \nabla \cdot \{\nabla\varphi, T\}$$
$$-\partial_y \left(\varphi + T\right) + \kappa_T \partial_y \nabla^2 \varphi = -\chi\nabla^4(a\varphi - bT), \tag{5}$$

$$\partial_t T + \{\varphi, T\} + \kappa_T \partial_y \varphi = \chi \nabla^2 T. \tag{6}$$

Viscosity and collisional coupling: $-\chi\nabla^4(a\varphi - bT)$

Normalised equations

$$\partial_t \left(\varphi' - \nabla^2\varphi\right) + \left\{\varphi, \varphi' - \nabla^2\varphi\right\} + \nabla \cdot \{\nabla\varphi, T\}$$
$$-\partial_y \left(\varphi + T\right) + \kappa_T \partial_y \nabla^2 \varphi = -\chi \nabla^4 (a\varphi - bT), \tag{5}$$

$$\partial_t T + \{\varphi, T\} + \kappa_T \partial_y \varphi = \chi \nabla^2 T. \tag{6}$$

Ion temperature perturbation: $\partial_t T$

Normalised equations

$$\partial_t \left(\varphi' - \nabla^2\varphi\right) + \left\{\varphi, \varphi' - \nabla^2\varphi\right\} + \nabla \cdot \{\nabla\varphi, T\}$$
$$-\partial_y \left(\varphi + T\right) + \kappa_T \partial_y \nabla^2 \varphi = -\chi \nabla^4 (a\varphi - bT), \tag{5}$$

$$\partial_t T + \{\varphi, T\} + \kappa_T \partial_y \varphi = \chi \nabla^2 T. \tag{6}$$

$\boldsymbol{E} \times \boldsymbol{B}$ advection of ion temperature: $\{\varphi, T\}$

Normalised equations

$$\partial_t \left(\varphi' - \nabla^2\varphi\right) + \left\{\varphi, \varphi' - \nabla^2\varphi\right\} + \nabla \cdot \{\nabla\varphi, T\}$$
$$-\partial_y \left(\varphi + T\right) + \kappa_T \partial_y \nabla^2 \varphi = -\chi \nabla^4 (a\varphi - bT), \tag{5}$$

$$\partial_t T + \{\varphi, T\} + \kappa_T \partial_y \varphi = \chi \nabla^2 T. \tag{6}$$

$\boldsymbol{E} \times \boldsymbol{B}$ advection of equilibrium temperature: $\kappa_T \partial_y \varphi$

Normalised equations

$$\partial_t \left(\varphi' - \nabla^2\varphi\right) + \left\{\varphi, \varphi' - \nabla^2\varphi\right\} + \nabla \cdot \{\nabla\varphi, T\}$$
$$-\partial_y \left(\varphi + T\right) + \kappa_T \partial_y \nabla^2 \varphi = -\chi \nabla^4 (a\varphi - bT), \tag{5}$$

$$\partial_t T + \{\varphi, T\} + \kappa_T \partial_y \varphi = \chi \nabla^2 T. \tag{6}$$

Thermal diffusion: $\chi \nabla^2 T$

ITG instability

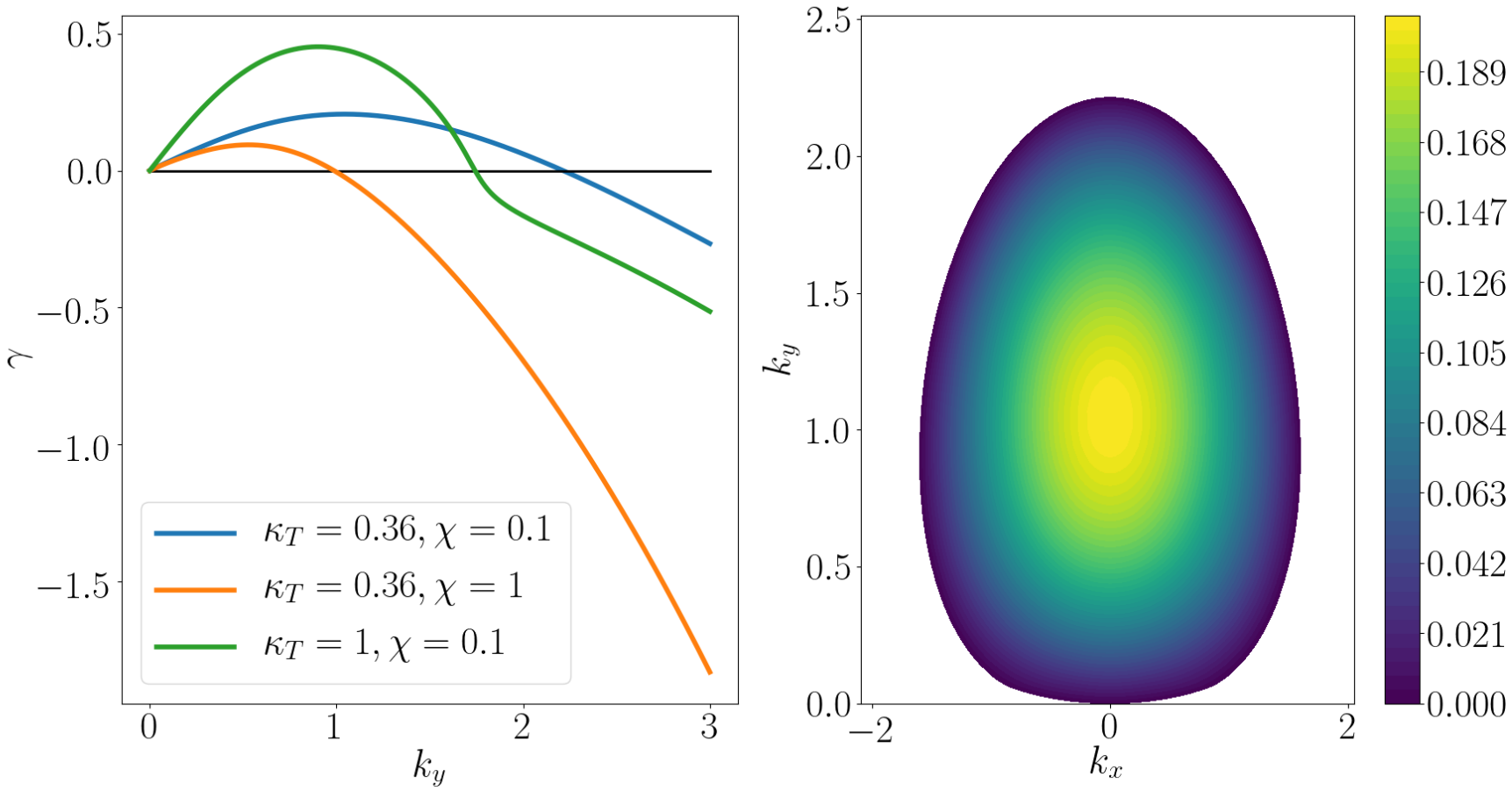

Figure 3: Linear growth rates of pure DW ($k_x = 0$) Fourier modes.

Saturated state

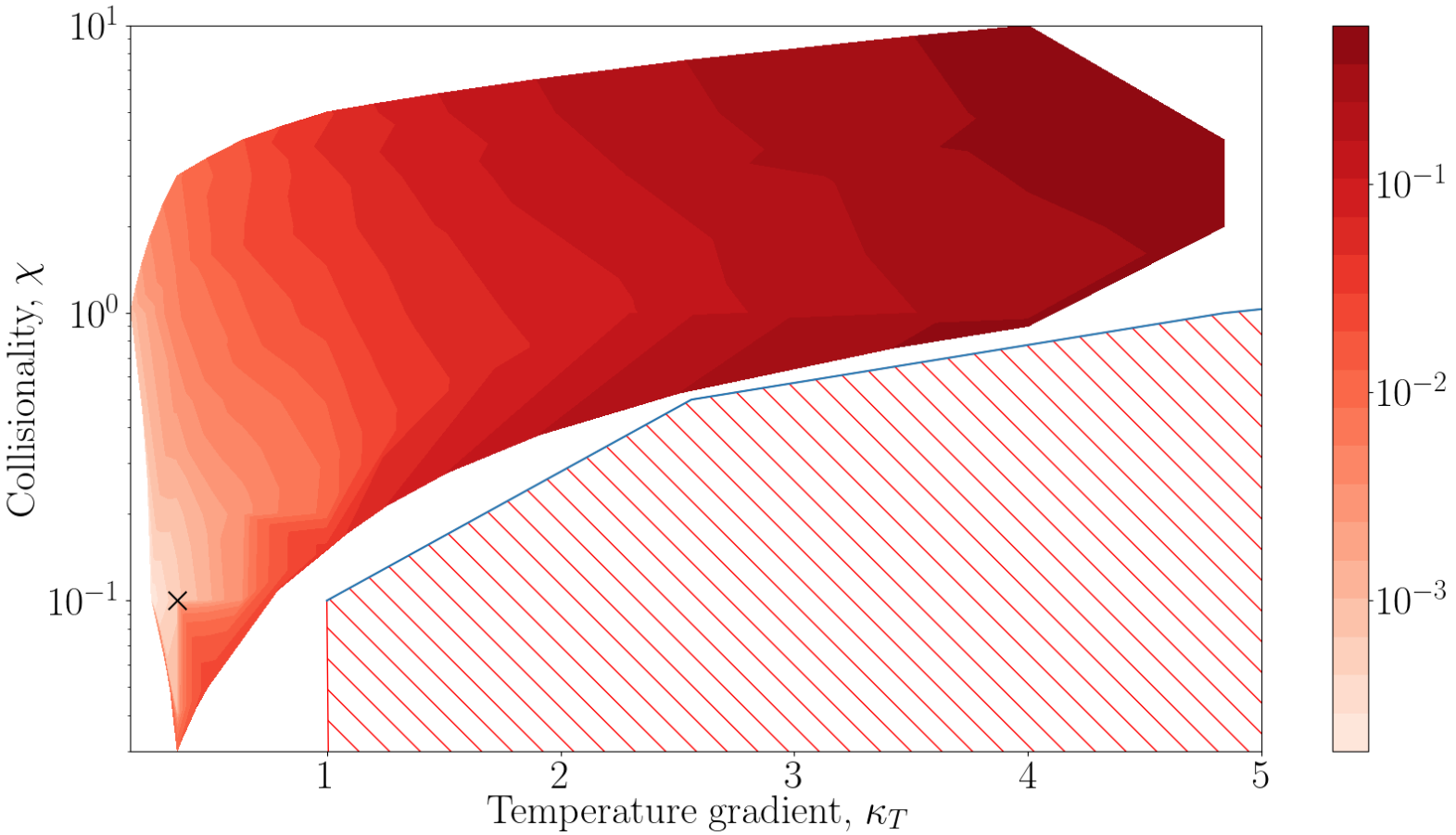

Figure 4: Log of the box-averaged heat flux $\ln Q$. The shaded region is beyond the Dimits threshold ($\kappa_T > \kappa_T^c$), where strong turbulence resides. The "X" marks the parameters $\kappa_T = 0.36, \chi = 0.1$, which we shall use to illustrate the near-marginal state.

Saturated state

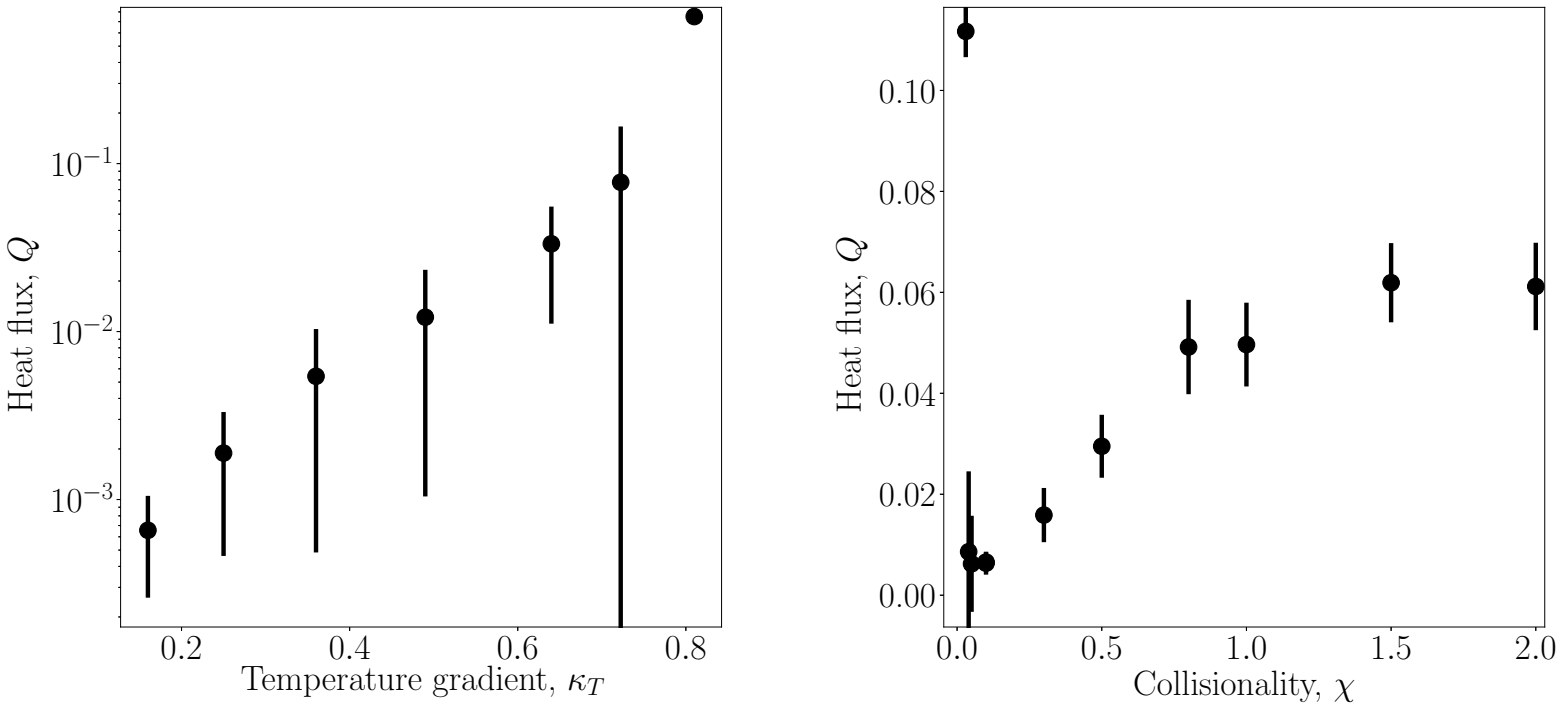

Figure 5: Left: Box-averaged heat flux Q in the saturated state versus κ_T for $\chi = 0.1$. Right: Box-averaged heat flux Q in the saturated state versus χ for $\kappa_T = 0.36$.

Near-marginal state

The near-marginal state is quasi-steady, occasionally interrupted by bursts of turbulence:

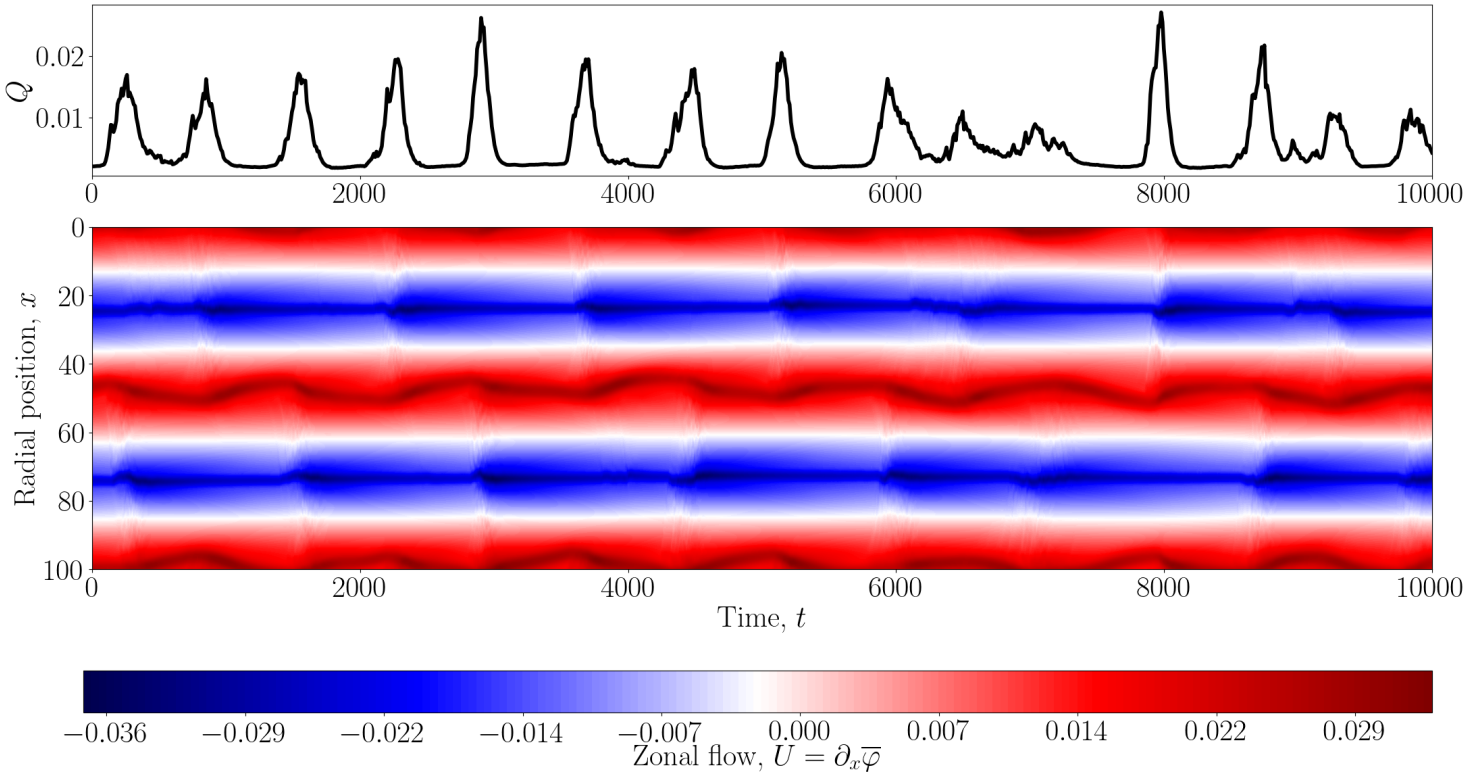

Figure 6: Top: time trace of the heat flux Q. Bottom: time trace of the ZF velocity, $U = \partial_x \overline{\varphi}$. Each turbulent burst is accompanied by an order-of-magnitude increase in Q.

Near-marginal state (between bursts)

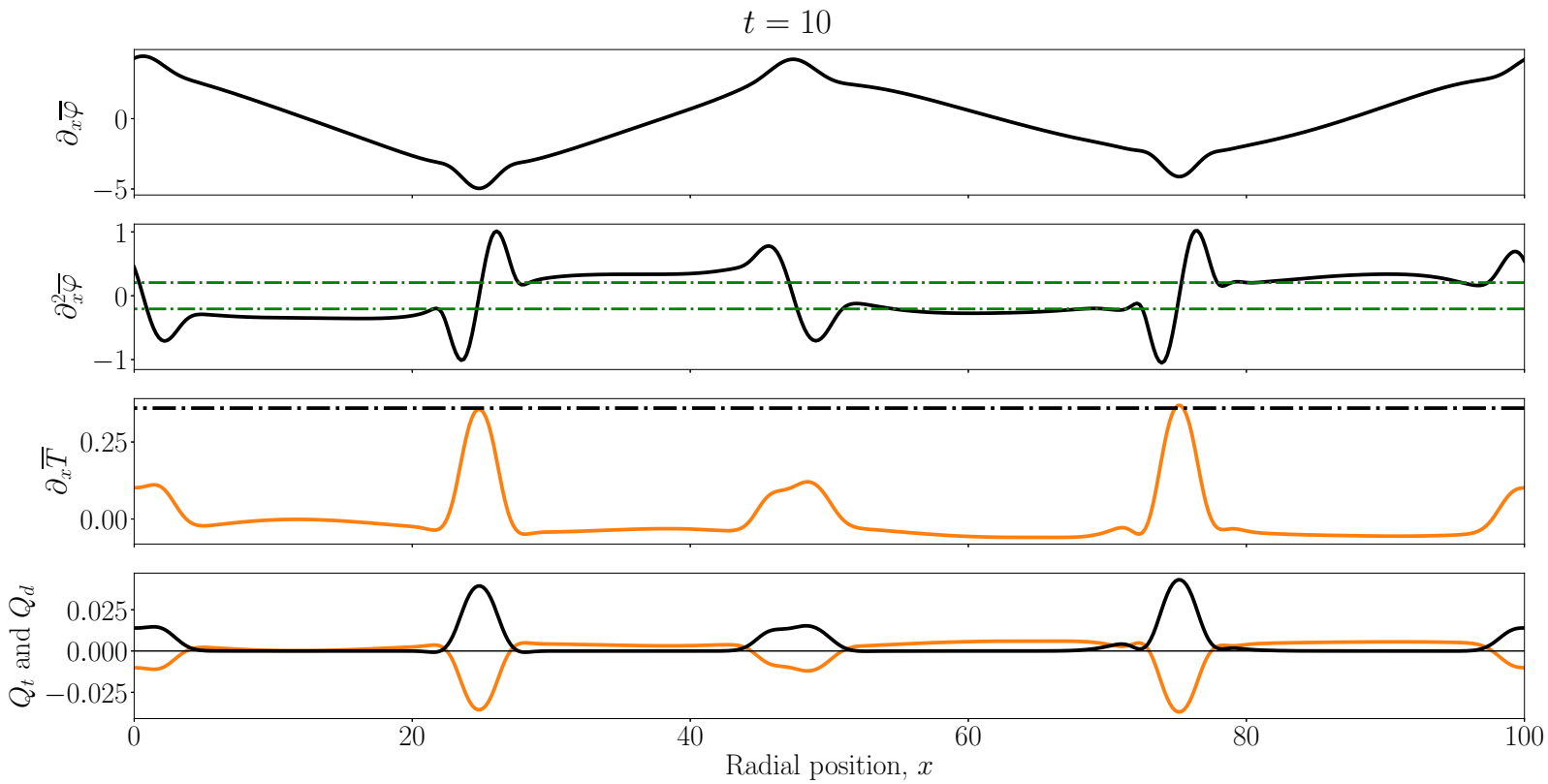

Figure 7: Radial profiles of ZF, zonal shear, zonal temperature gradient, turbulent (black) and diffusive (orange) radial heat fluxes. The dashed green line corresponds to the largest linear ITG growth rate $\pm\gamma_{\max}$. The dashed black line shows the value of the equilibrium temperature gradient κ_T. Here $\kappa_T = 0.36, \chi = 0.1$.

Turbulent bursts

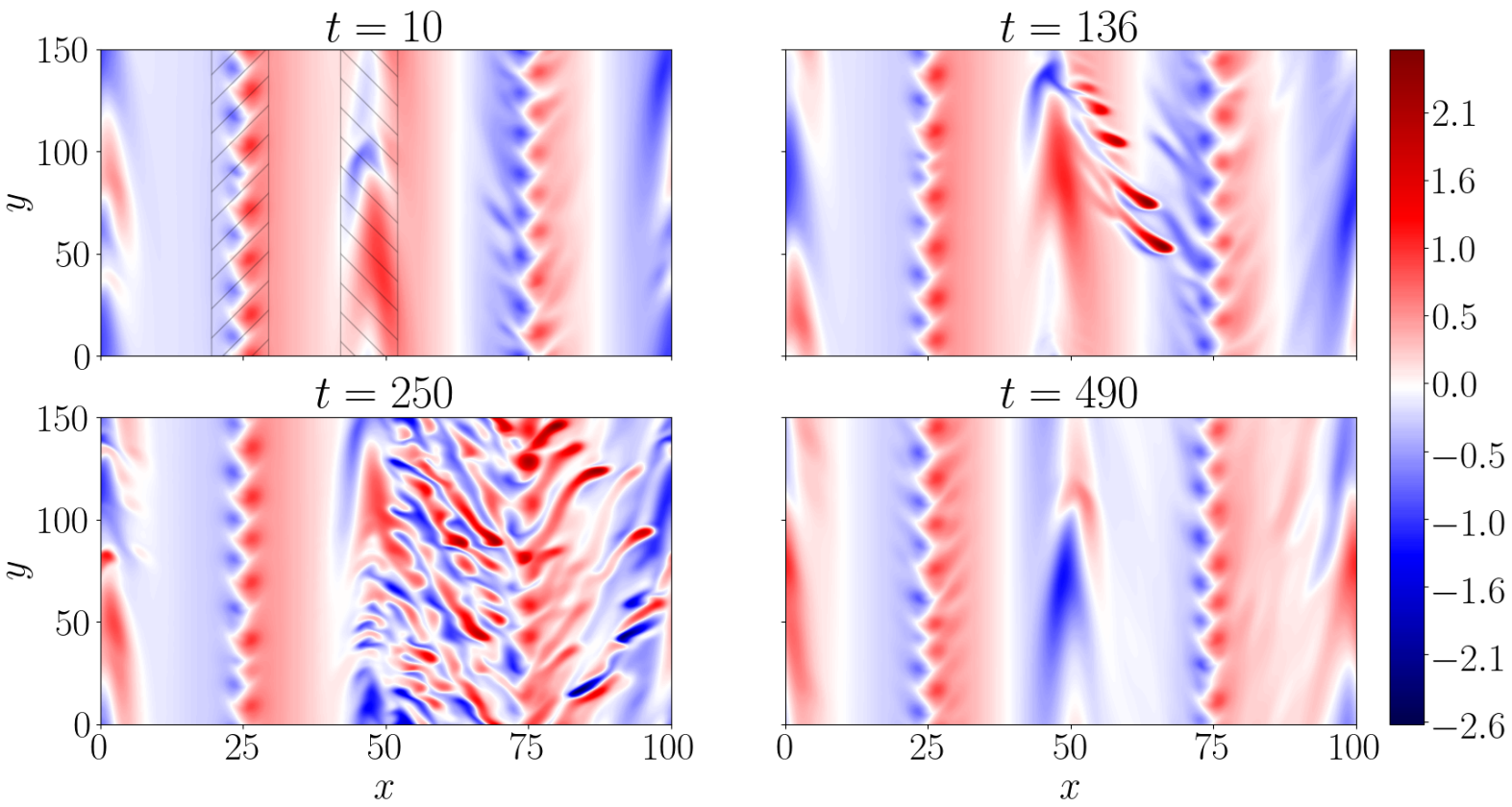

Figure 8: Temperature perturbations before, during, and after a turbulent burst for $\chi = 0.1, \kappa_T = 0.36$. The shaded areas on the top-left panel mark the ZF minimum around $x = 25$ and maximum around $x = 47$.

Momentum flux

- Let us investigate the way in which zonal profiles are reconstituted after the turbulent bursts. The equation for $\overline{\varphi}$ is
$$\partial_t \overline{\varphi} = \overline{\partial_x \varphi \partial_y (\varphi + T)} + \chi \partial_x^2 (a\overline{\varphi} - b\overline{T}). \tag{7}$$
- Define the Reynolds stress $\Pi_\varphi \equiv \overline{\partial_x \varphi \partial_y \varphi}$ and the "diamagnetic" stress $\Pi_T \equiv \overline{\partial_x \varphi \partial_y T}$
- These two comprise the turbulent momentum flux that drives the ZFs
- Numerically we find that Π_φ and Π_T have opposite signs

Momentum flux

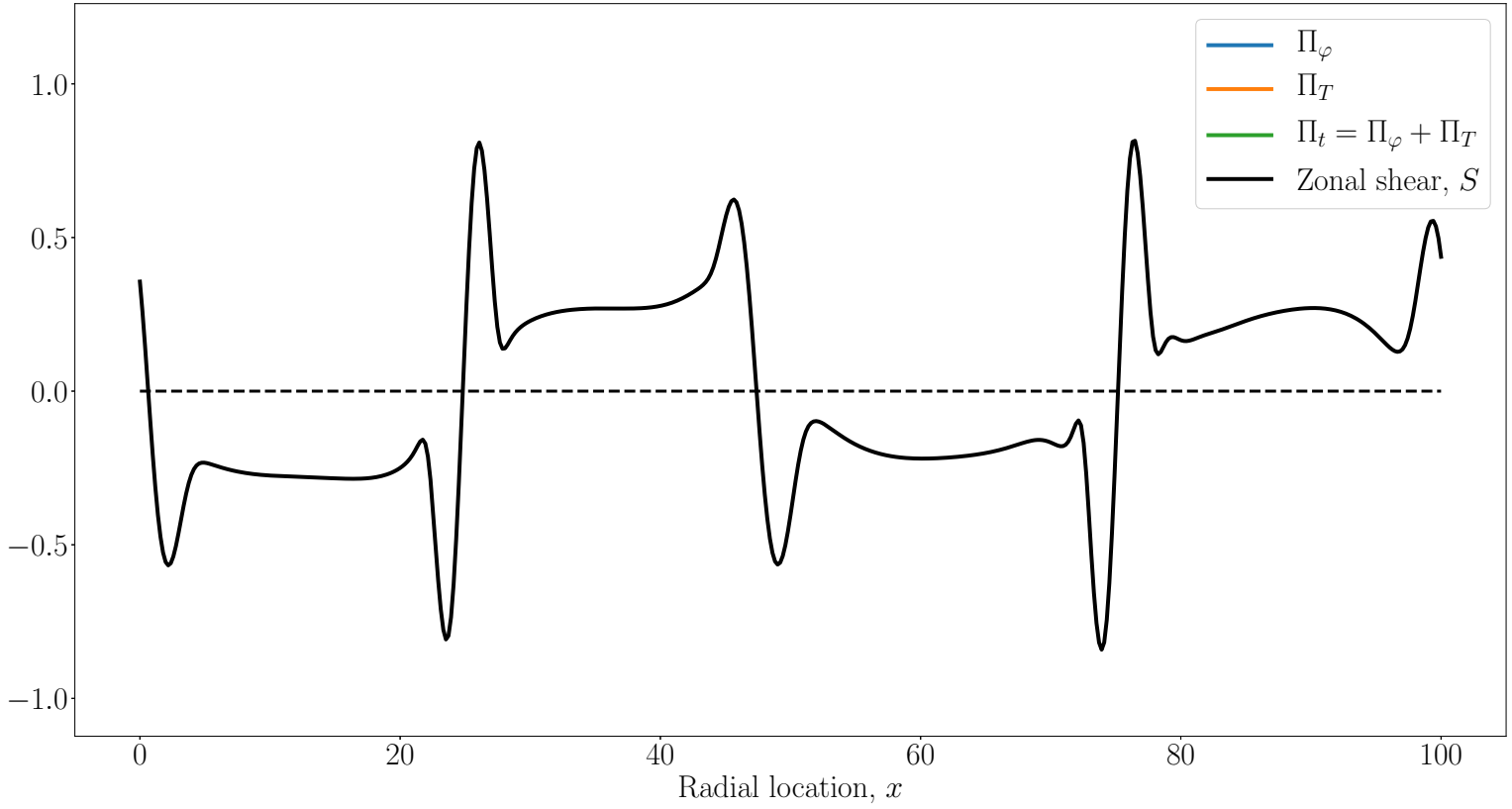

Figure 9: Time-averaged momentum fluxes for saturated ITG turbulence over a fixed zonal background. The sign of $\Pi_t = \Pi_\varphi + \Pi_T$ coincides with that of Π_φ and opposes the sign of S. This reflects that $\kappa_T = 0.36 < \kappa_T^c \approx 1$.

Momentum flux

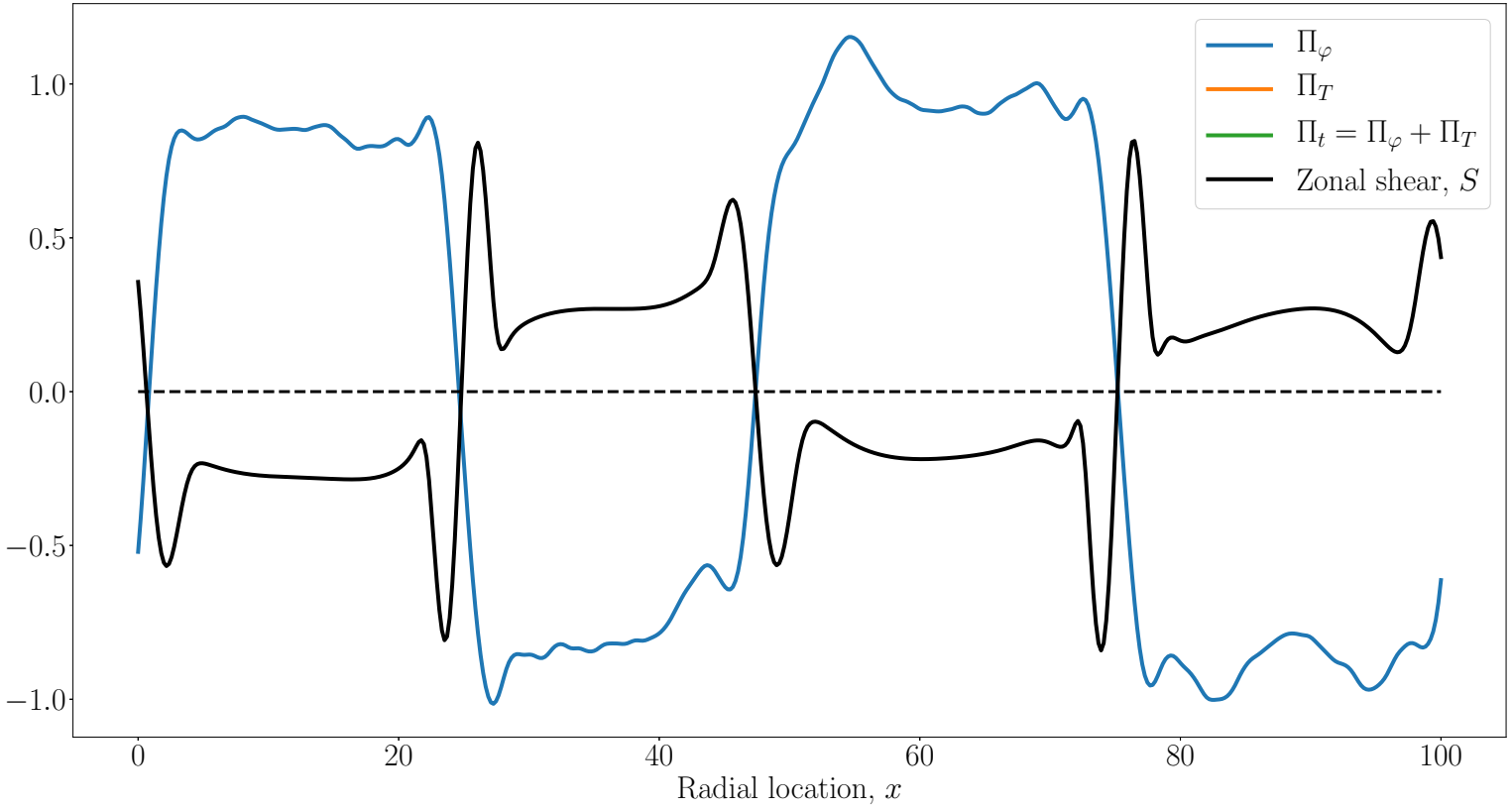

Figure 9: Time-averaged momentum fluxes for saturated ITG turbulence over a fixed zonal background. The sign of $\Pi_t = \Pi_\varphi + \Pi_T$ coincides with that of Π_φ and opposes the sign of S. This reflects that $\kappa_T = 0.36 < \kappa_T^c \approx 1$.

Momentum flux

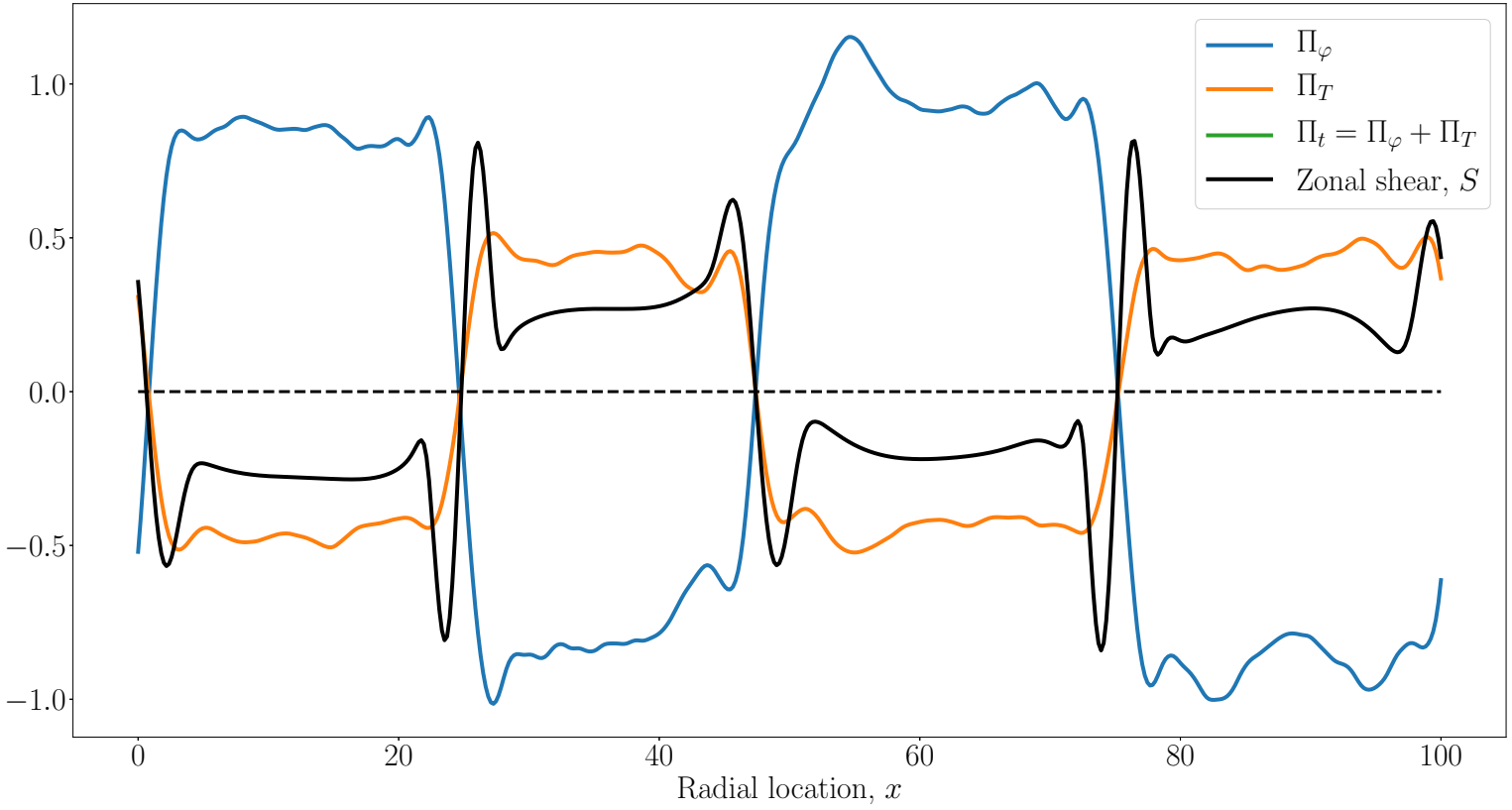

Figure 9: Time-averaged momentum fluxes for saturated ITG turbulence over a fixed zonal background. The sign of $\Pi_t = \Pi_\varphi + \Pi_T$ coincides with that of Π_φ and opposes the sign of S. This reflects that $\kappa_T = 0.36 < \kappa_T^c \approx 1$.

Momentum flux

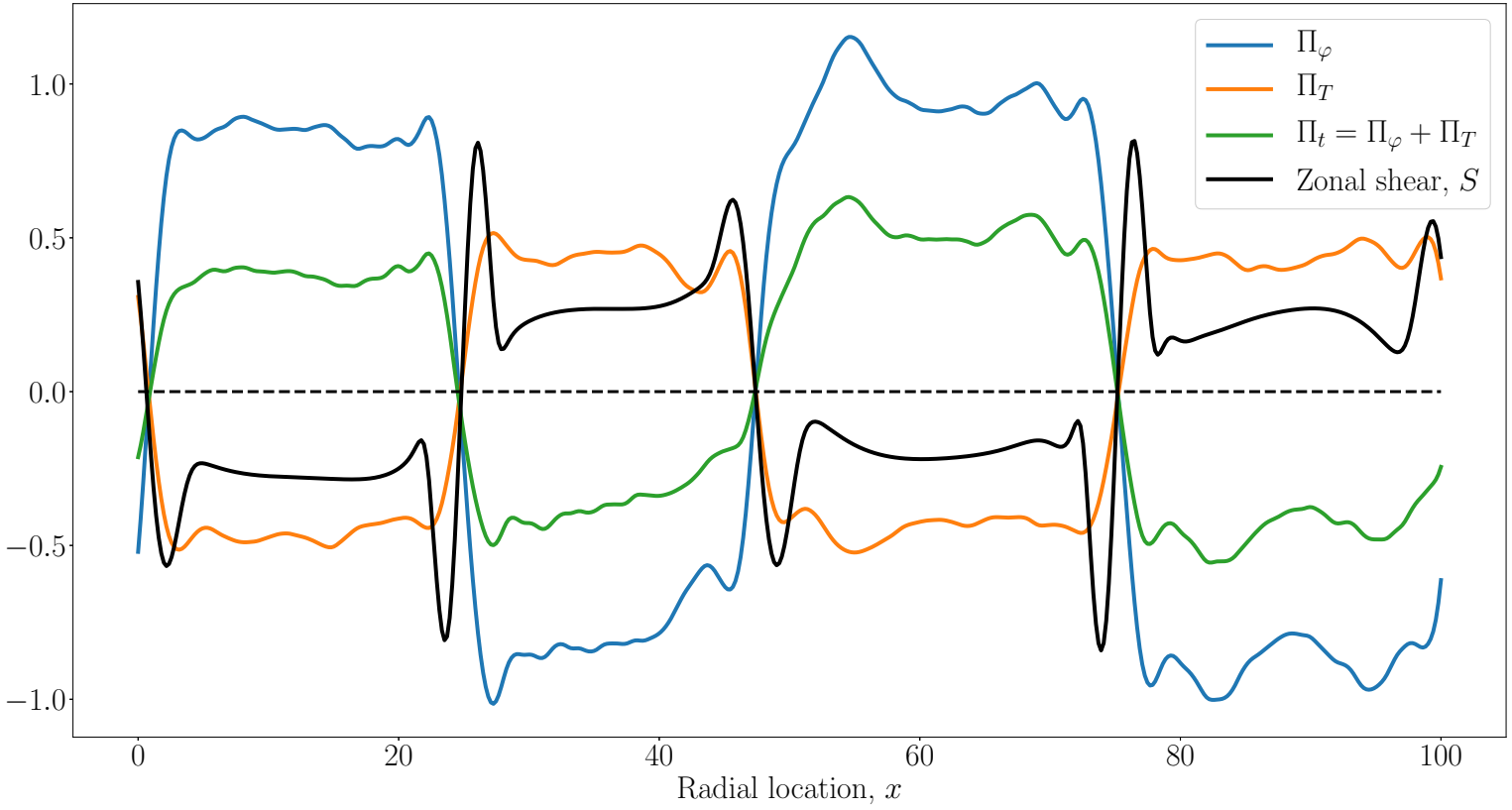

Figure 9: Time-averaged momentum fluxes for saturated ITG turbulence over a fixed zonal background. The sign of $\Pi_t = \Pi_\varphi + \Pi_T$ coincides with that of Π_φ and opposes the sign of S. This reflects that $\kappa_T = 0.36 < \kappa_T^c \approx 1$.

Momentum flux

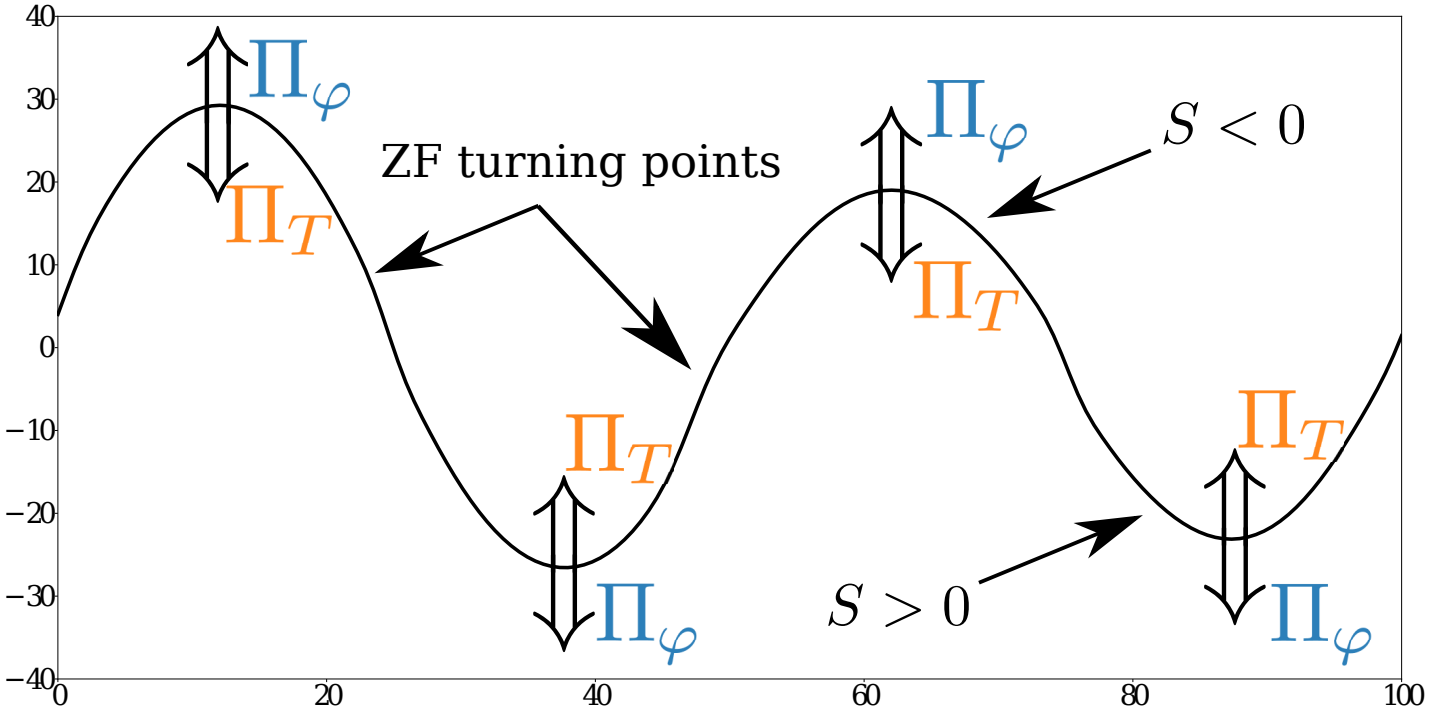

Figure 10: An illustration of the enhancing and diminishing effects of Π_φ and Π_T on the ZF. The black curve is the zonal electrostatic potential φ.

$$\partial_t \overline{\varphi} = \Pi_\varphi + \Pi_T + \text{viscosity}$$

Momentum flux for constant ZF shear

- We can understand the effect of the zonal shear by changing coordinates to the "shearing frame":

$$t' = t,\ x' = x,\ y' = y - Stx. \tag{8}$$

- A Fourier mode in the shearing frame corresponds to a lab-frame mode with a time-dependent radial wavenumber:

$$k_x = k'_x - Stk'_y,\ k_y = k'_y. \tag{9}$$

- Thus, $S > 0$ anticorrelates the signs of k_x and k_y, and vice-versa for $S < 0$

Momentum flux for constant ZF shear

- We can integrate the Reynolds stress:

$$\int \frac{dx}{L_x}\, \Pi_\varphi = \int \frac{dx}{L_x}\, \overline{\partial_x \varphi \partial_y \varphi} = \sum_{\boldsymbol{k}} k_x k_y |\varphi_k|^2 \qquad (10)$$

- For $S > 0$ we get $k_x k_y < 0$ on average (due to $k_x = k'_x - Stk'_y$), and vice-versa for $S < 0$
- Thus S and Π_φ have opposite signs

Momentum flux for constant ZF shear

- We can write a similar expression for the diamagnetic stress:

$$\frac{1}{L_x}\int dx\ \Pi_T = \sum_{\boldsymbol{k}} k_x k_y |\varphi_{\boldsymbol{k}}|^2 \mathrm{Re}\frac{T_{\boldsymbol{k}}}{\varphi_{\boldsymbol{k}}}. \tag{11}$$

- Then the total turbulent momentum flux is

$$\frac{1}{L_x}\int dx\ (\Pi_\varphi + \Pi_T) = \sum_{\boldsymbol{k}} k_x k_y |\varphi_{\boldsymbol{k}}|^2 \left(1 + \mathrm{Re}\frac{T_{\boldsymbol{k}}}{\varphi_{\boldsymbol{k}}}\right). \tag{12}$$

- Hence a (k_x, k_y) mode feeds the ZFs if and only if $\mathrm{Re}(T_k/\varphi_k) > -1$

Momentum flux for constant ZF shear

- The term $\mathrm{Re}(T_{\boldsymbol{k}}/\varphi_{\boldsymbol{k}})$ is hard to predict analytically
- We can get a good heuristic understanding using the linear modes
- It turns out that $\mathrm{Re}(T_{\boldsymbol{k}}/\varphi_{\boldsymbol{k}}) < 0$ for all linear modes

Varying κ_T

What happens to the ITG turbulence over an imposed static ZF when we vary the temperature gradient κ_T?

Varying κ_T

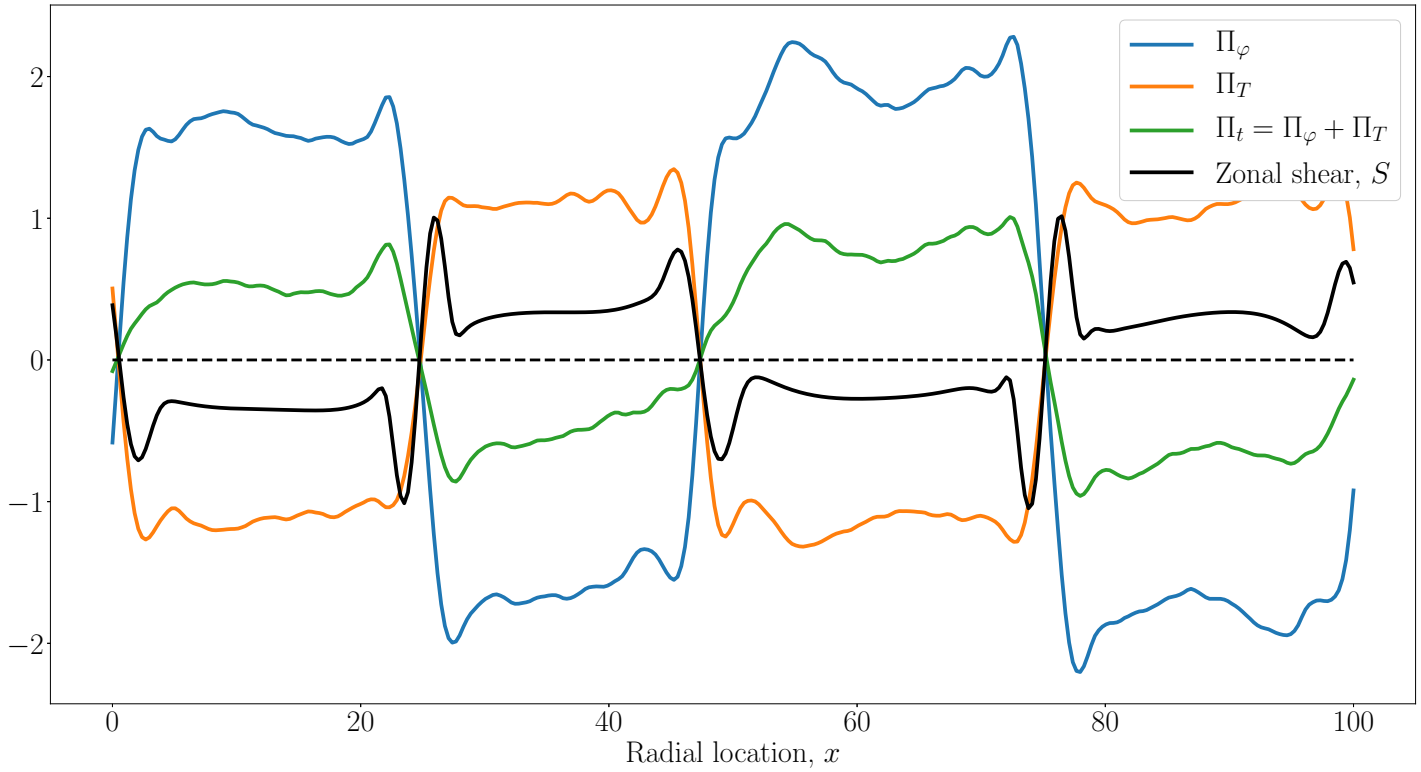

Figure 11: Time-averaged momentum fluxes for saturated ITG turbulence over a fixed zonal background, $\kappa_T = 0.49, \chi = 0.1$.

Varying κ_T

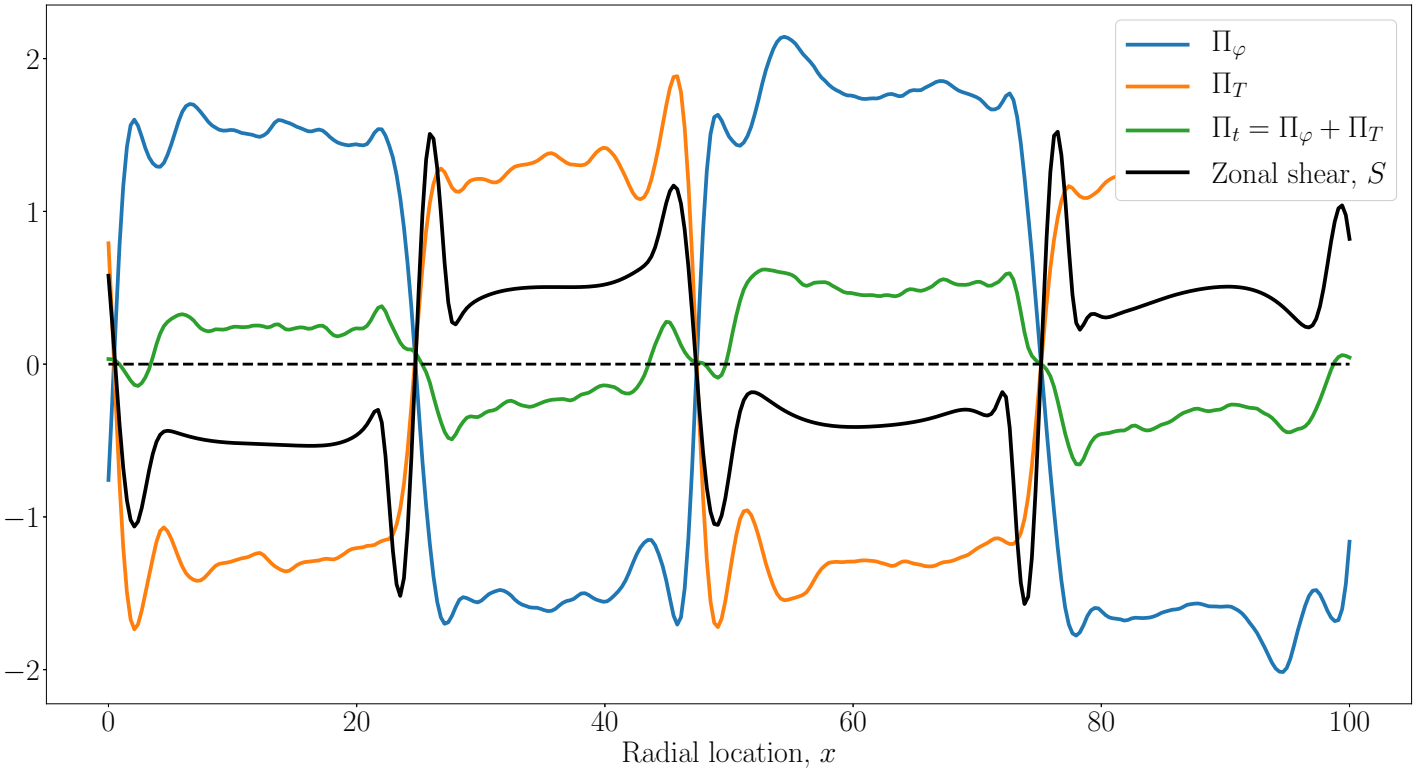

Figure 11: Time-averaged momentum fluxes for saturated ITG turbulence over a fixed zonal background, $\kappa_T = 0.64, \chi = 0.1$.

Varying κ_T

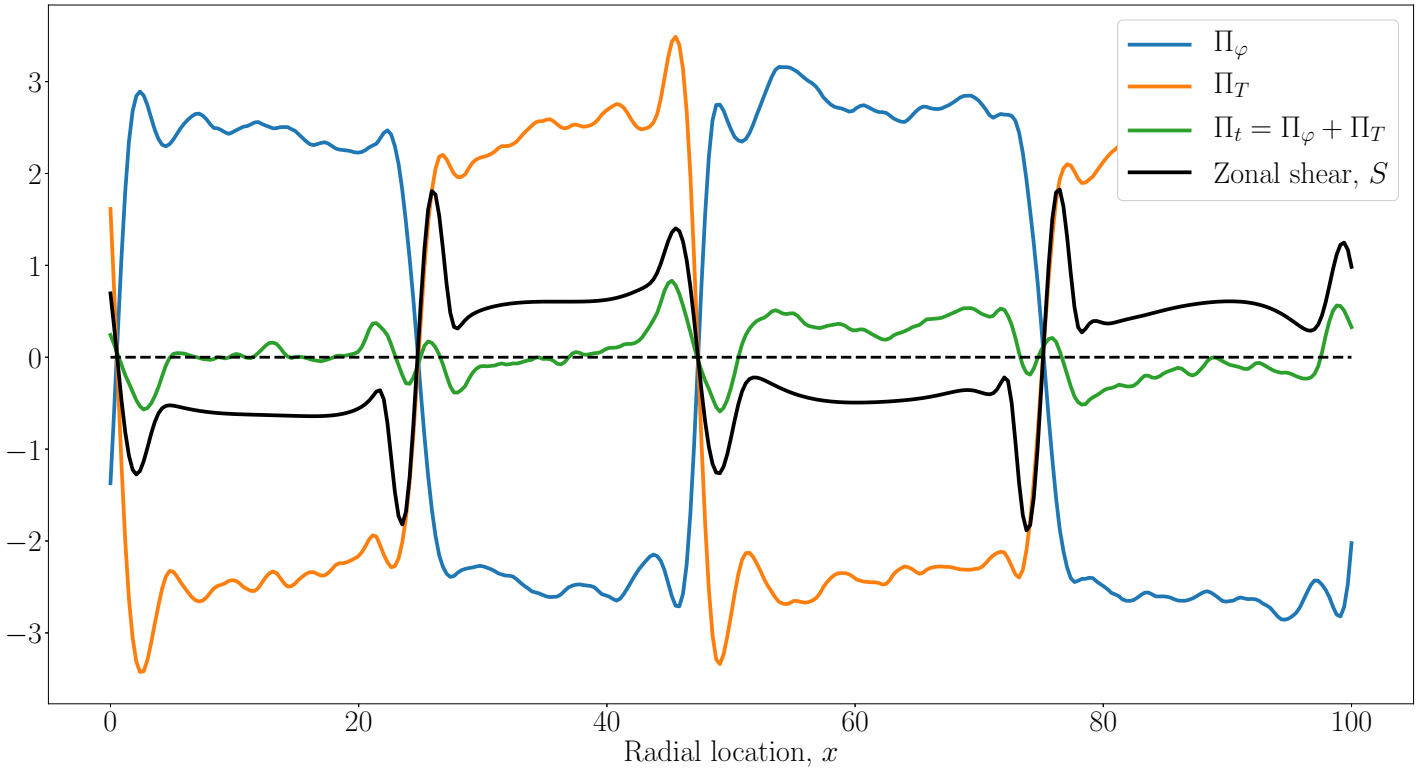

Figure 11: Time-averaged momentum fluxes for saturated ITG turbulence over a fixed zonal background, $\kappa_T = 0.81, \chi = 0.1$.

Varying κ_T

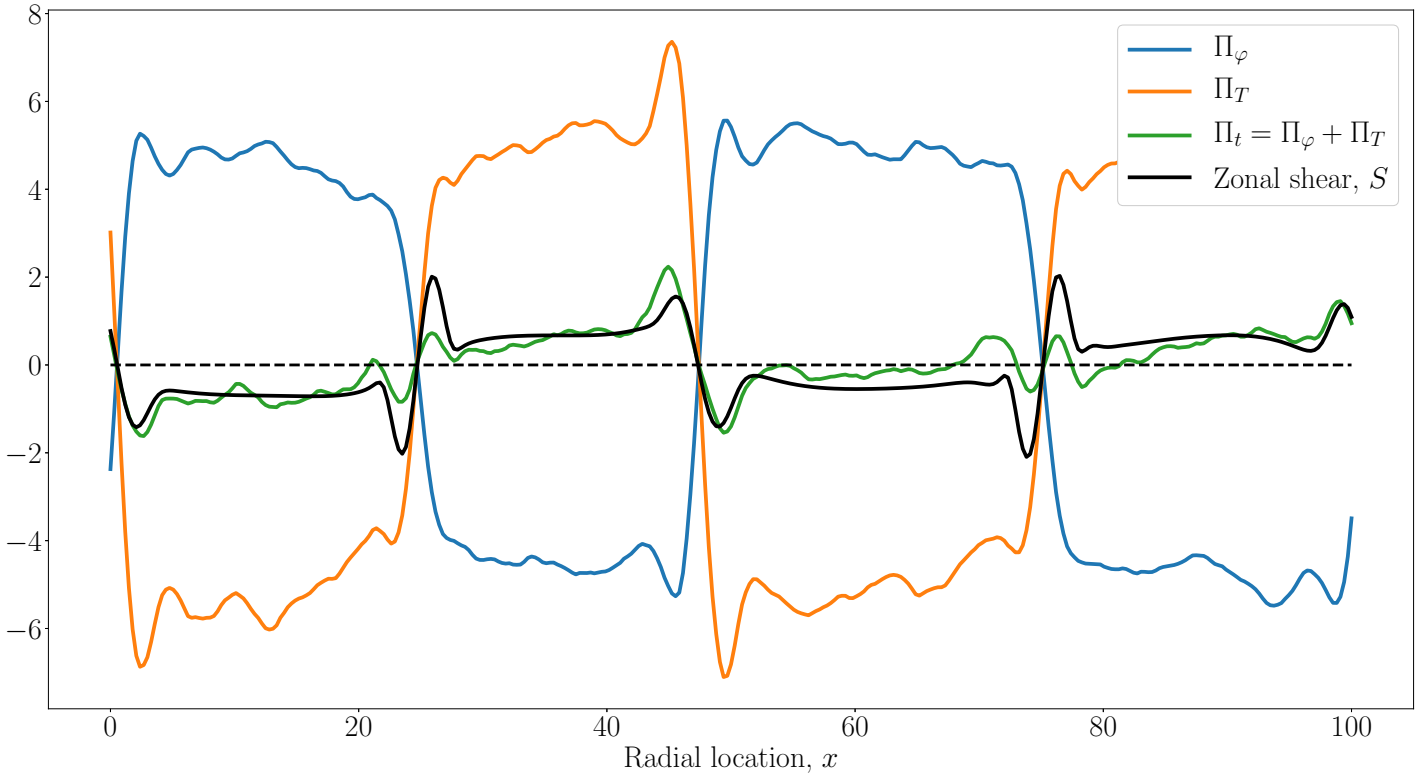

Figure 11: Time-averaged momentum fluxes for saturated ITG turbulence over a fixed zonal background, $\kappa_T = 1, \chi = 0.1$.

Varying κ_T

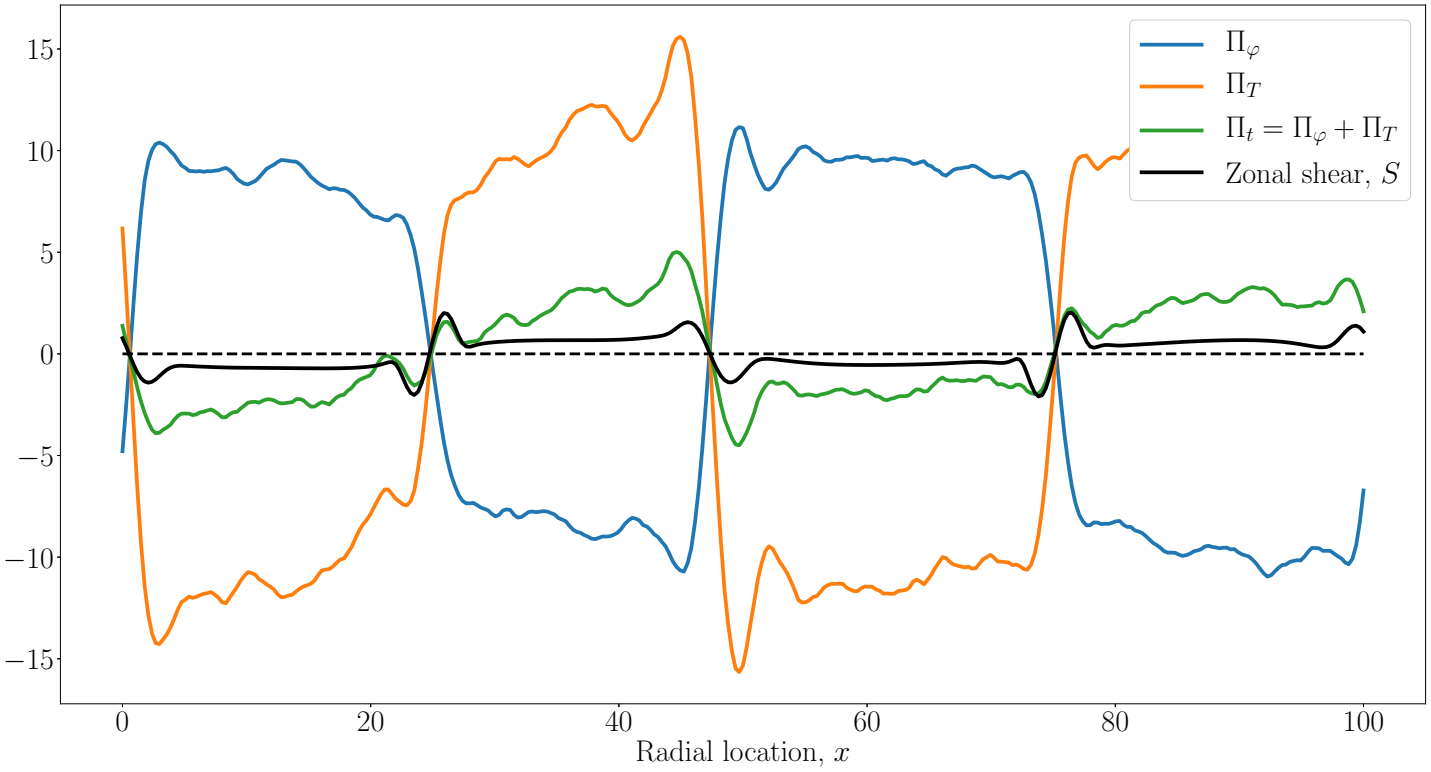

Figure 11: Time-averaged momentum fluxes for saturated ITG turbulence over a fixed zonal background, $\kappa_T = 1.21, \chi = 0.1$.

Varying κ_T

- We can vary the temperature gradient κ_T at fixed χ and a fixed static ZF profile
- It turns out that as κ_T increases, so does Π_T relative to Π_φ
- Denote by κ_T^{static} the gradient at which the Reynolds and diamagnetic stresses balance in order to give a time-averaged $\Pi_t = \Pi_\varphi + \Pi_T \approx 0$
- The value of κ_T^{static} is found to be insensitive to the exact ZF profile used and coincides with the observed Dimits threshold κ_T^c

Linear mode approximation for the Dimits threshold

- We can use the linear mode structure to approximate κ_T^{static}, and, by extension, κ_T^c
- We look for κ_T such that $\text{Re}(T_k/\varphi_k) = -1$ for the "appropriate" modes
- The most unstable modes in general are streamers ($k_x = 0$), but these cannot survive the strong ZFs
- We use the most unstable mode with $k_x = k_y$

Linear mode approximation for the Dimits threshold

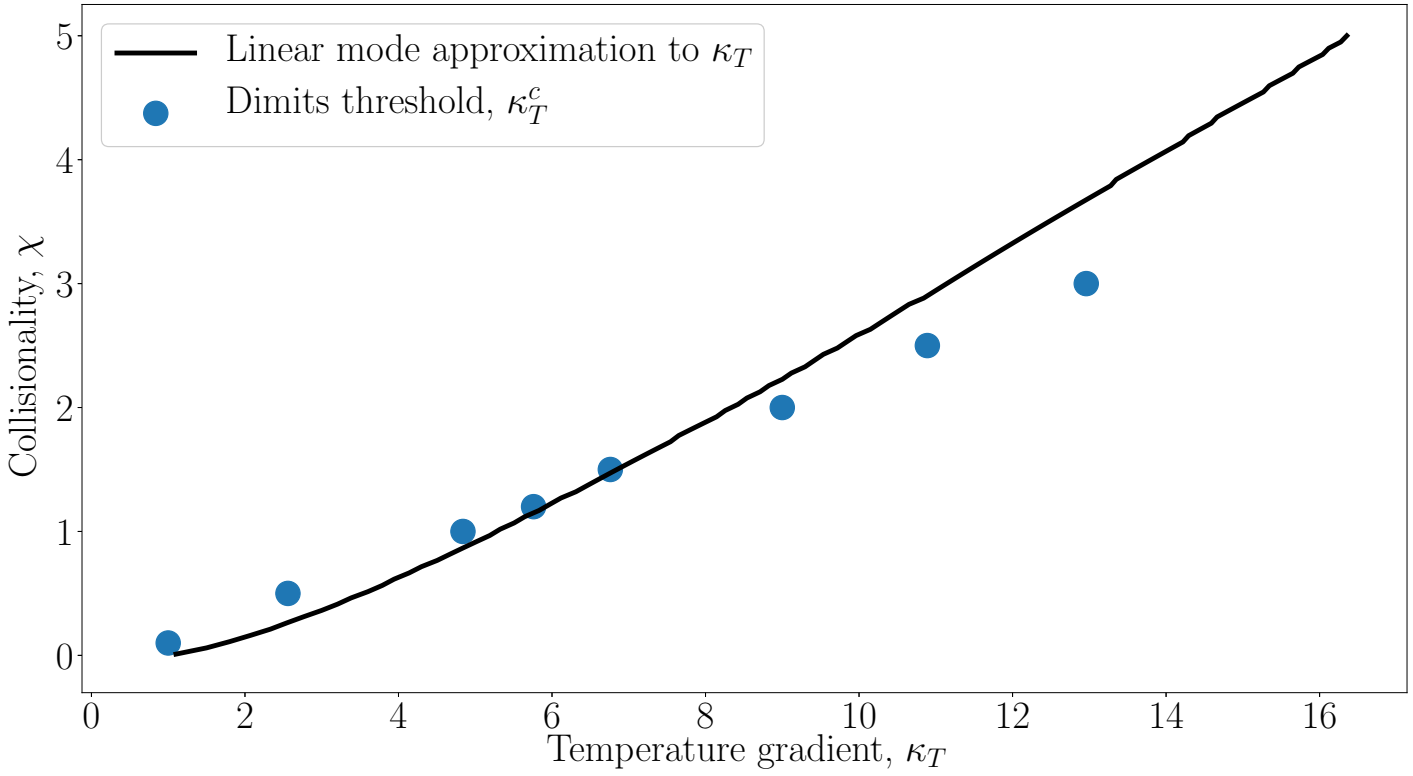

Figure 12: Comparison of numerical data (blue points) and analytic approximation (black curve) for the Dimits threshold.

Conclusions

- We have described the Dimits regime for curvature-driven ITG turbulence in 2D
- The ZFs and zonal temperature work together to suppress the instability in two different ways — strong zonal shear and temperature-gradient flattening
- Occasional tubulent bursts occur due to the viscous decay of the ZFs
- The Dimits threshold is linked to the turbulent momentum flux of ITG turbulence over an imposed ZF shear
- We proposed and verified a quantitative formula for the value of the Dimits threshold

Acknowledgements

The author would like to thank M. R. Hardman, D. A. St-Onge, I. Y. Dodin, and the Oxford Plasma Theory group for useful discussions.

P.G.I. is funded through an EU H2020 grant, agreement No 3000207035. This work has been carried out within the framework of the EUROfusion Consortium and has received funding from the Euratom research and training programme 2014-2018 and 2019-2020 under grant agreement No 633053. The views and opinions expressed herein do not necessarily reflect those of the European Commission.

Normalisations

$$\hat{t} \equiv \frac{2\rho_s \Omega_i}{L_B} t, \qquad \hat{x} \equiv \frac{x}{\rho_s}, \qquad \hat{y} \equiv \frac{y}{\rho_s},$$

$$\hat{\varphi} \equiv \frac{\tau L_B \varphi}{2\rho_s} = \frac{\tau L_B}{2\rho_s} \frac{Z_i e \phi}{T_i}, \qquad \hat{T} \equiv \frac{\tau L_B T}{2\rho_s} = \frac{\tau L_B}{2\rho_s} \frac{\delta T}{T_i}, \tag{13}$$

$$\kappa_T \equiv \frac{\tau L_B}{2L_T}, \qquad \hat{\chi} \equiv \frac{\tau L_B}{\rho_s} \frac{8}{9} \sqrt{\frac{2}{\pi}} \frac{\nu_i}{\Omega_i},$$

$$[Q] = \frac{3}{\tau^{3/2}\sqrt{2}} n_i T_i v_{ti} \left(\frac{\rho_i}{L_B} \right)^2. \tag{14}$$

Near-marginal state (between bursts)

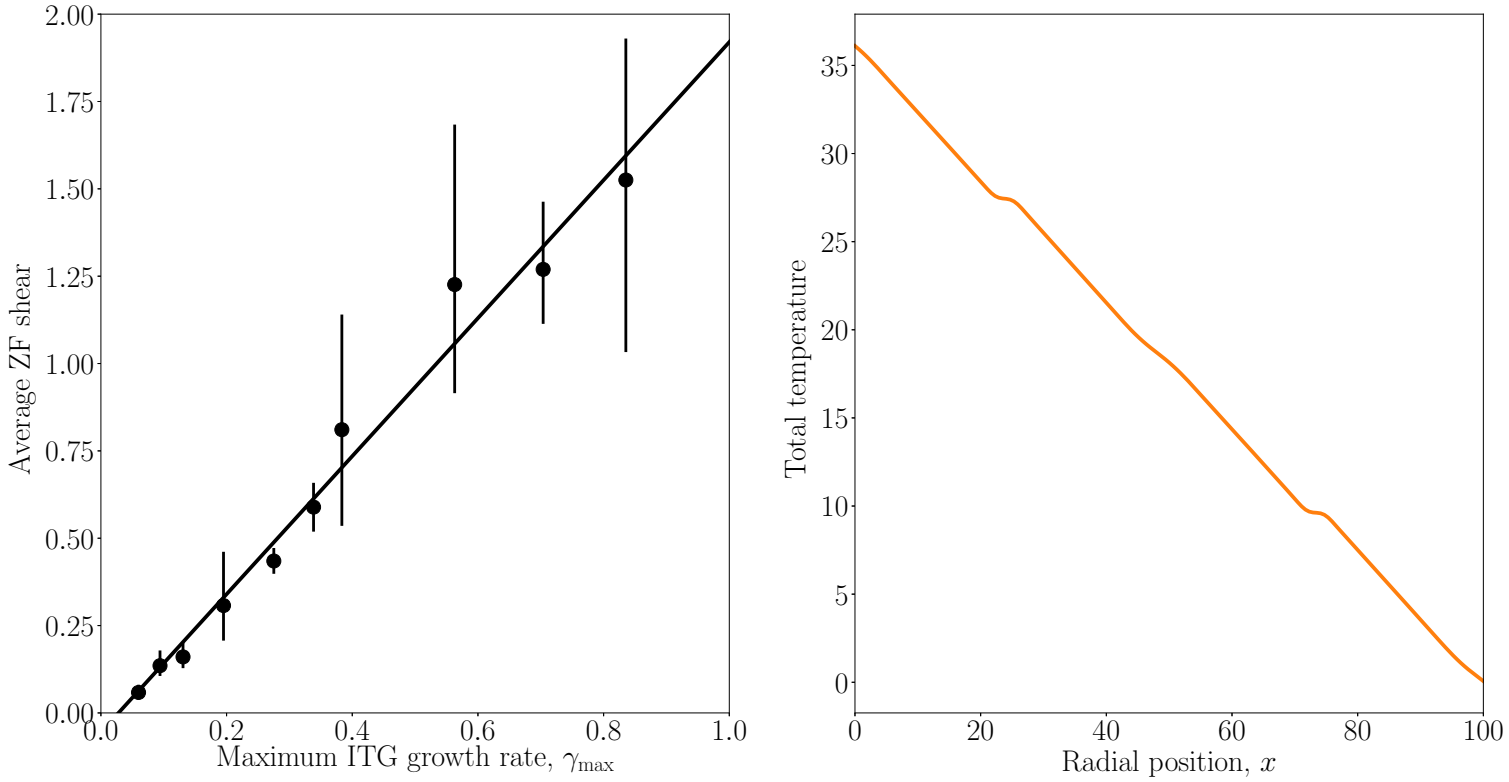

Figure 13: Left: Time- and space-averaged over the shear zones ZF shear S versus maximum ITG growth rate $\gamma_{\max}$. The fitted line is $S \approx 2\gamma_{\max}$. Right: Time-averaged of normalised total temperature relative to the absolute temperature T_R of the right edge of the domain.

Near-marginal state

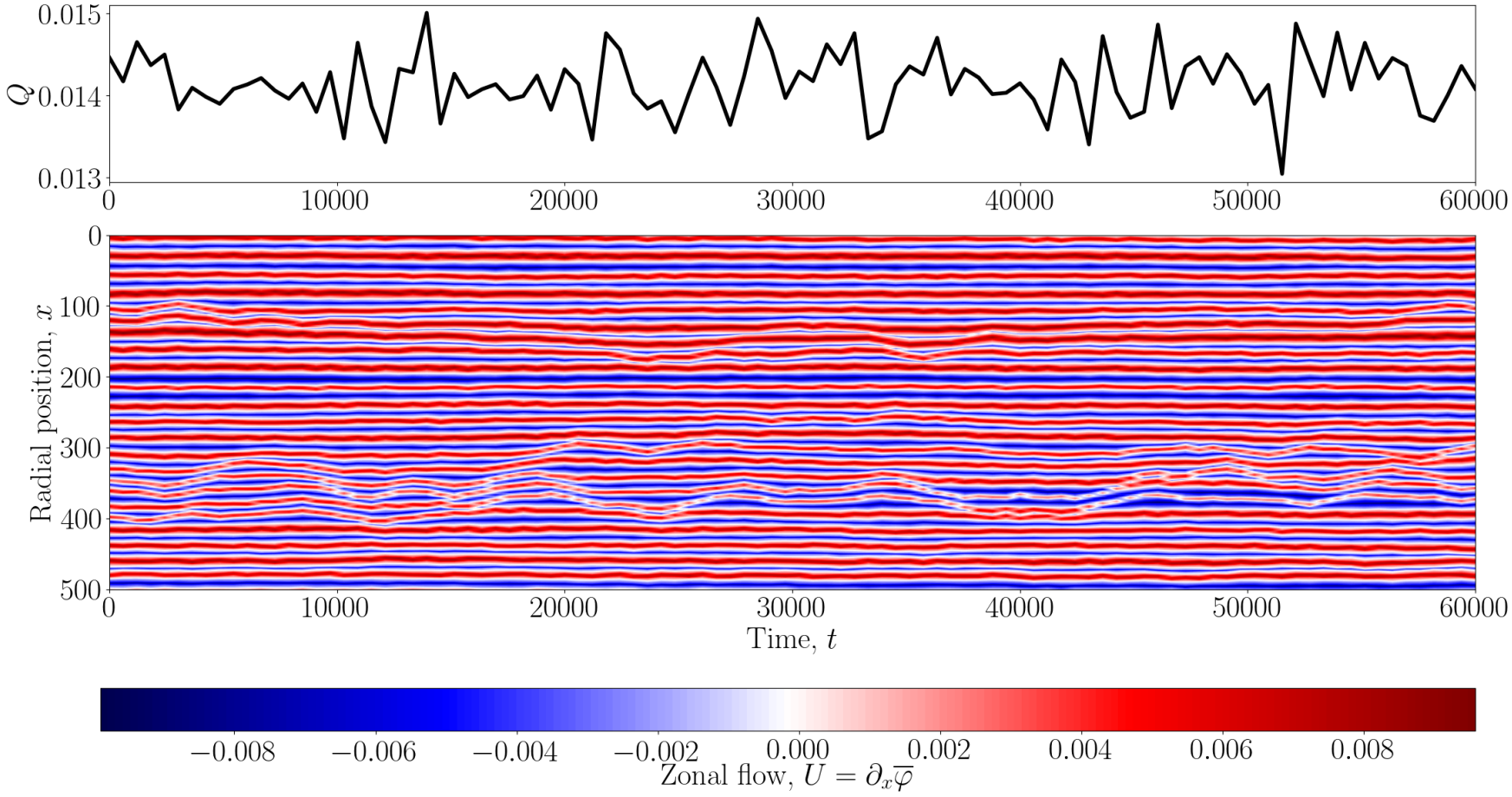

Figure 14: .

Beyond the threshold

- Beyond the staircase state, our equations fail to reach saturation
- The transition from ZF-dominated saturation to blow-up in this system is equivalent to the transition from the zonally-dominated Dimits regime to fully developed turbulence
- Saturation in GK simulations beyond Dimits is "critically balanced" (Barnes *et al.*, 2011), hence fundamentally 3D

Blow up

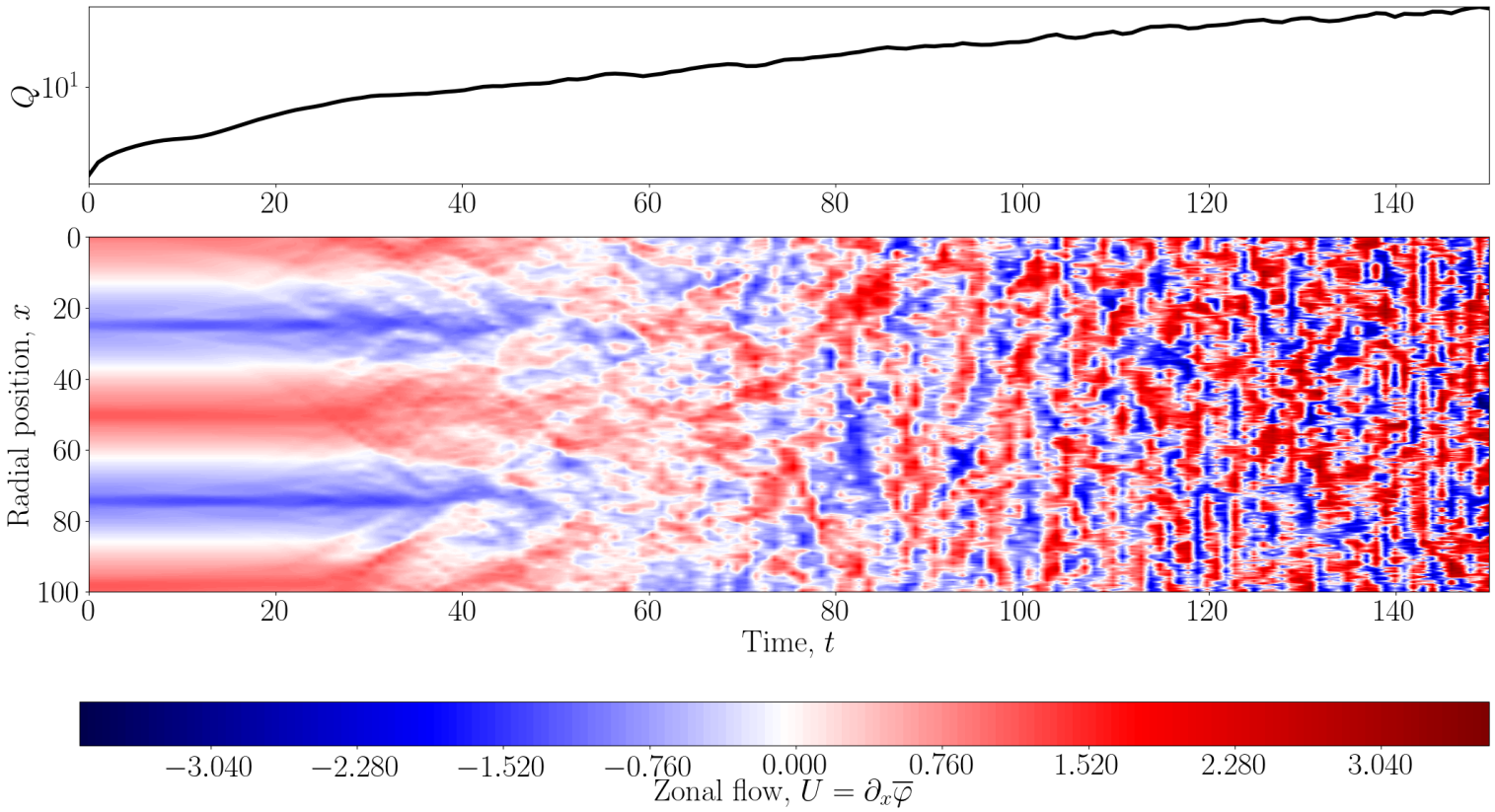

Figure 15: Heat flux evolution beyond the Dimits regime.

Blow up

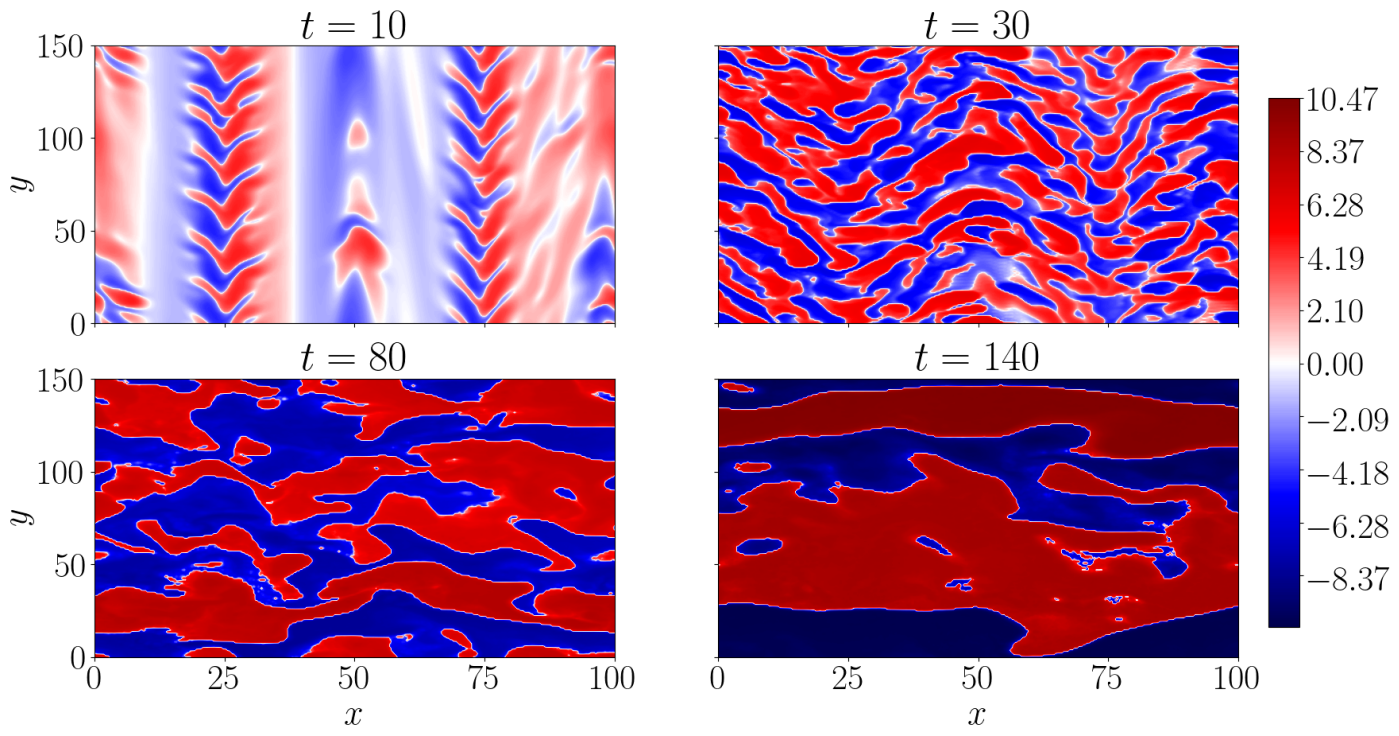

Figure 16: Snapshots of temperature perturbations in the blow up state beyond the Dimits threshold. The colours actually represent $\operatorname{arcsinh}(10T)$ in order to visualise properly the vast difference in amplitudes.

Turbulent bursts

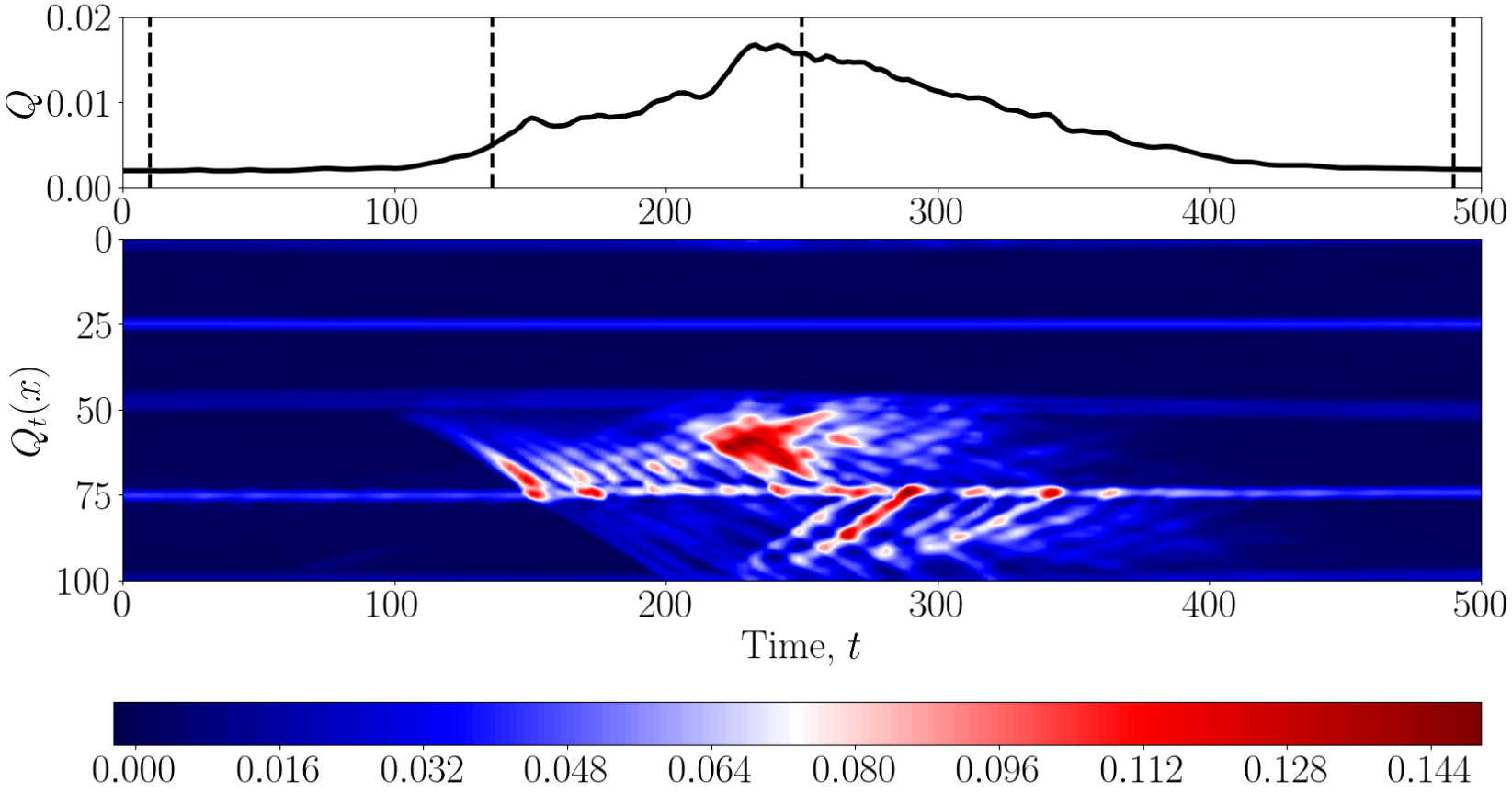

Figure 17: A close view of a turbulent burst. Top: time trace of the box-integrated radial heat flux Q. Bottom: time trace of the local radial heat flux.

Localised Structures

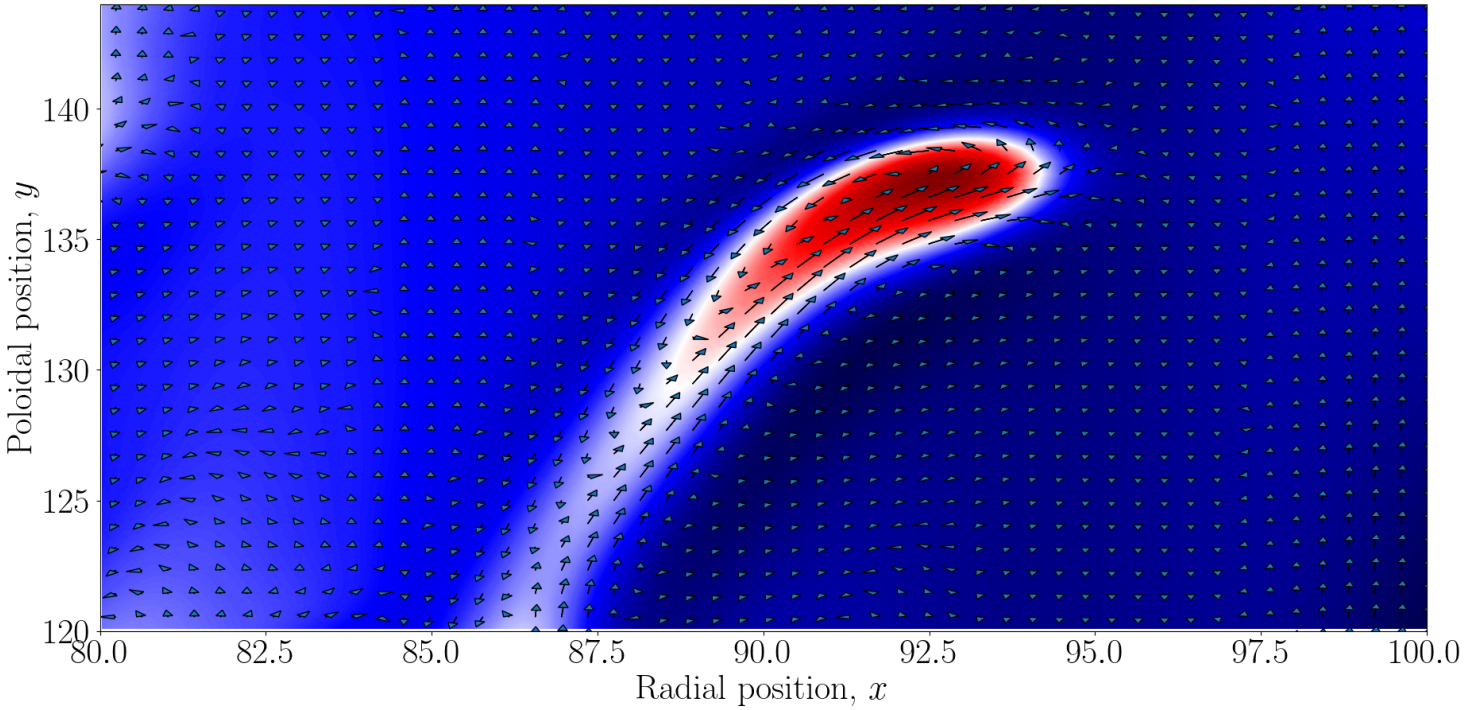

Figure 18: Snapshot of T with structures visible.

- Soliton-like "ferdinons" (van Wyk *et al.*, 2016) are seen drifting through the sheared regions
- These structures increase the heat flux dramatically
- They trigger the turbulent bursts

Localised Structures

- These structures can drift both inwards and outwards, regardless of the local zonal shear
- The direction of their radial drift is given by their net temperature
- They are always emitted from ZF maxima
- GK avalanches with similar properties have been reported by Villard *et al.* (2013)

Localised Structures

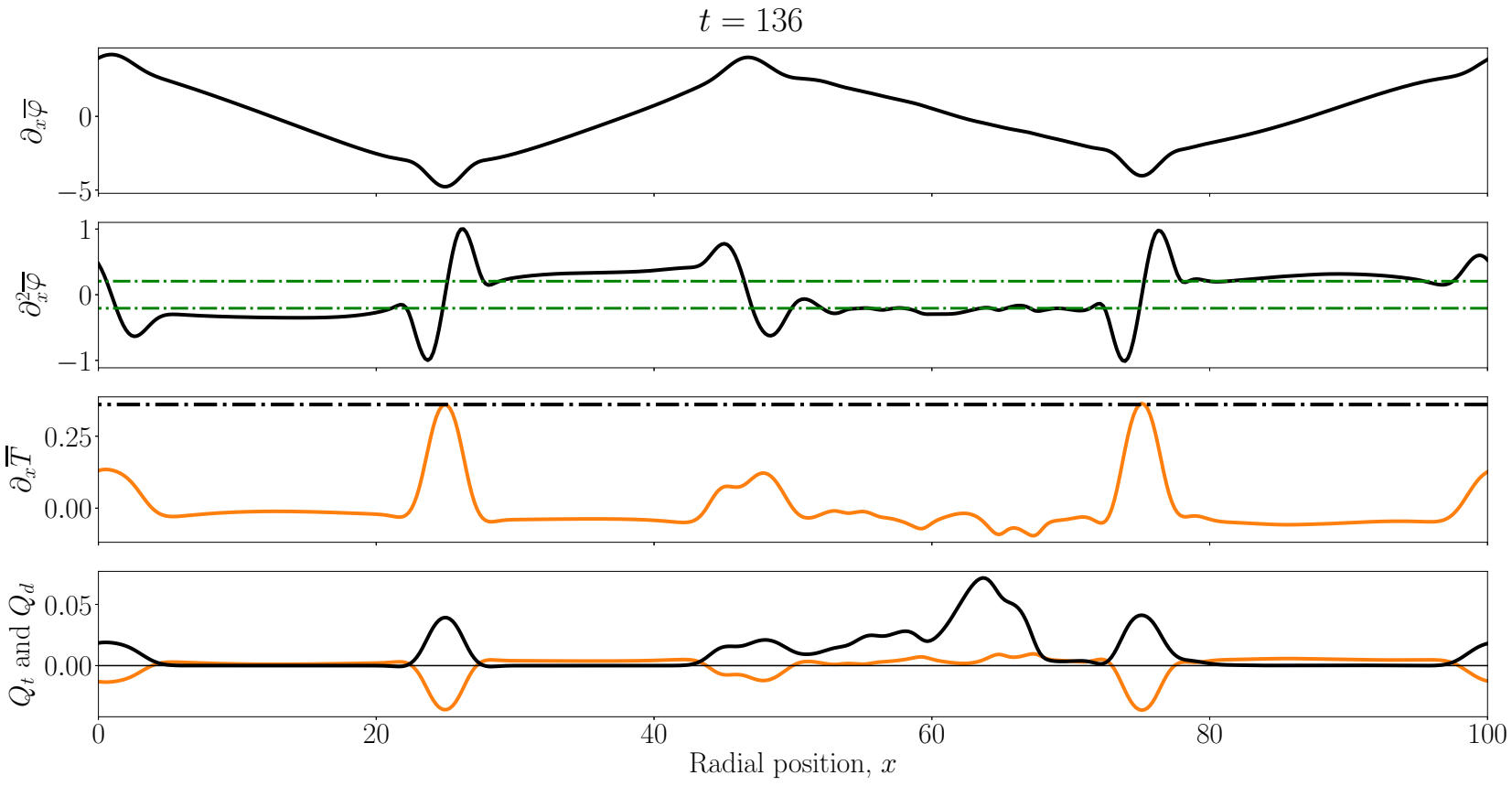

Figure 19: Similar to a previous figure, but right after ferdinons have been created.

Influence of ZFs on turbulent perturbations

Let us highlight the terms, where the ZF enters the equations:

$$
\begin{aligned}
&(\partial_t \boldsymbol{+U\partial_y})\left(1-\nabla^2\right)\varphi' - (1\boldsymbol{-\partial_x^3\overline{\varphi}})\partial_y\left(\varphi'+T'\right) + \kappa_T\partial_y\nabla^2\varphi' \\
&\quad \boldsymbol{+S\partial_x\partial_y T'} + \left\{\varphi', -\nabla^2\varphi'\right\} + \nabla\cdot\left\{\nabla\varphi', T\right\} \\
&\quad = -\chi\nabla^4(a\varphi' - bT'),
\end{aligned}
\tag{15}
$$

$$
(\partial_t \boldsymbol{+U\partial_y})T + \kappa_T\partial_y\varphi + \left\{\varphi', T\right\} = \chi\nabla^2 T, \tag{16}
$$

where $U = \partial_x\overline{\varphi}$ and $S = \partial_x^2\overline{\varphi}$.

Barnes, M, Parra, FI & Schekochihin, AA 2011 Critically balanced ion temperature gradient turbulence in fusion plasmas. *Physical Review Letters* **107**, 115003.

Dif-Pradalier, G., Diamond, P. H., Grandgirard, V., Sarazin, Y., Abiteboul, J., Garbet, X., Ghendrih, Ph., Strugarek, A., Ku, S. & Chang, C. S. 2010 On the validity of the local diffusive paradigm in turbulent plasma transport. *Phys. Rev. E* **82**, 025401.

Dimits, AM, Cohen, BI, Mattor, N, Nevins, WM, Shumaker, DE, Parker, SE & Kim, C 2000 Simulation of ion temperature gradient turbulence in tokamaks. *Nuclear Fusion* **40** (3Y), 661.

Hammett, GW, Beer, MA, Dorland, W, Cowley, SC & Smith, SA 1993 Developments in the gyrofluid approach to tokamak turbulence simulations. *Plasma Physics and Controlled Fusion* **35** (8), 973.

Villard, L, Angelino, P, Bottino, A, Brunner, S, Jolliet, S, McMillan, B F, Tran, T M & Vernay, T

2013 Global gyrokinetic ion temperature gradient turbulence simulations of ITER. *Plasma Physics and Controlled Fusion* **55** (7), 074017.

van Wyk, F., Highcock, E. G., Schekochihin, A. A., Roach, C. M., Field, A. R. & Dorland, W. 2016 Transition to subcritical turbulence in a tokamak plasma. *Journal of Plasma Physics* **82** (6), 905820609.